Bioconjugate Chemistry

Review

Cite This: *Bioconjugate Chem.* 2020, 31, 315−331

pubs.acs.org/bc

Biodegradable Inorganic Nanoparticles for Cancer Theranostics: Insights into the Degradation Behavior

Hui Zhou,[†,#] Jianxian Ge,[†,#] Qingqing Miao,[†] Ran Zhu,[†] Ling Wen,[‡] Jianfeng Zeng,[*,†] and Mingyuan Gao[†,§]

[†]Center for Molecular Imaging and Nuclear Medicine, State Key Laboratory of Radiation Medicine and Protection, School for Radiological and Interdisciplinary Sciences (RAD-X), Soochow University, Collaborative Innovation Center of Radiological Medicine of Jiangsu Higher Education Institutions, Suzhou 215123, China

[‡]Department of Radiology, The First Affiliated Hospital of Soochow University, Suzhou 215006, China

[§]Institute of Chemistry, Chinese Academy of Sciences/School of Chemistry and Chemical Engineering, University of Chinese Academy of Sciences, Beijing 100190, China

ABSTRACT: Inorganic nanoparticles as a versatile nanoplatform have been broadly applied in the diagnosis and treatment of cancers due to their inherent superior physicochemical properties (including magnetic, thermal, optical, and catalytic performance) and excellent functions (e.g., imaging, targeted delivery, and controlled release of drugs) through surface functional modification or ingredient dopant. However, in practical biological applications, inorganic nanomaterials are relatively difficult to degrade and excrete, which induces a long residence time in living organisms and thus may cause adverse effects, such as inflammation and tissue cysts. Therefore, the development of biodegradable inorganic nanomaterials is of great significance for their biomedical application. This Review will focus on the recent advances of degradable inorganic nanoparticles for cancer theranostics with highlight on the degradation mechanism, aiming to offer an in-depth understanding of degradation behavior and related biomedical applications. Finally, key challenges and guidelines will be discussed to explore biodegradable inorganic nanomaterials with minimized toxicity issues, facilitating their potential clinical translation in cancer diagnosis and treatment.

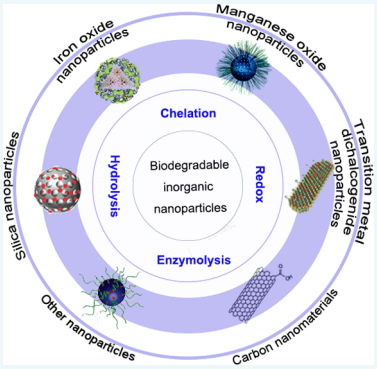

1. INTRODUCTION

In the past few decades, nanoparticles as a biomedical application platform have attracted increasing attention,[1−6] and several of them (e.g., liposomes[7] and albumin[8]) have been successfully applied in clinical practice, indicating their great potential in nanomedicine. After systemic administration, however, most of the artificial nanoparticles are recognized by the immune system of organism and then captured by the reticuloendothelial system (RES, e.g., liver and spleen),[9−12] leading to long-term retention in the body and potential toxicity, which largely hampers their practical application. According to the requirements of the Food and Drug Administration (FDA), agents injected into the human body, especially diagnostic ones, must be completely cleared within a reasonable period of time after achieving the purpose.[13] Thus, nanoparticles with effectively clearable properties have more clinical translation opportunities.

Biodegradation and renal clearance are considered as the two major pathways that can accelerate the removal of nanoparticles from the body.[13−24] It is demonstrated that ultrasmall nanoparticles with hydrodynamic size less than 5.5 nm can be rapidly excreted through renal pathway.[13,24−28] However, rapid renal clearance largely shortens the circulation time *in vivo* and thus reduces the time available for the nanoparticles to perform their functions. Additionally, although the renal clearance can eliminate a large proportion of the administrated ultrasmall nanoparticles, the accumulation and retention in the body cannot be completely avoided. Compared with the ultrasmall nanoparticles, nanoparticles with larger size (e.g., 20−200 nm) not only have longer residence time in the bloodstream, but also provide more space for functionalization, such as targeted molecule modification and drug loading.[29] However, the declining kidney filtration makes the nanoparticles more prone to accumulate in RES, resulting in increased challenge of potential toxicity in biological system.[25,30,31] Therefore, a more promising approach is to develop appropriately sized and degradable nanoplatforms, which enable sufficient time to perform diagnostic or therapeutic functions, and then decompose into small pieces of degradation products that can be utilized by the organism or removed from the body.[26,32]

Generally, biodegradable nanoparticles can be divided into three categories, including inorganic nanoparticles (e.g., silica, iron oxide, transition metal dichalcogenide, and metal

Special Issue: Molecular Imaging

Received: October 16, 2019
Revised: November 24, 2019
Published: November 25, 2019

DOI: 10.1021/acs.bioconjchem.9b00699
Bioconjugate Chem. 2020, 31, 315−331

Table 1. Degradation Mechanism and Degradation Behavior of Represented Inorganic Nanoparticles[a]

degradation mechanism	nanoparticle	size	degradation behavior	ref
Hydrolysis	DOX-LPSiNPs	151 nm	completely degraded and cleared from the body within 4 weeks	29
	BLM-SiO_2−BLM	80 nm	completely collapse into fragments after incubated in water for 16 days	78
	PEG-SiO_2 NP	3.4 nm	almost completely degraded after coincubated with cells for 7 days	79
	PEG-SiO_2 NP	118 nm	fully degraded and cleared from body within 3 months	80
Chelation	Iron oxide nanocubes	21 nm	quickly degraded within 1 h after being incubated in citrate medium of pH 4.7	65
	Iron-doped silica Nanoshells	200 nm	nearly completely degraded after being exposed to FBS or HS containing transferrin for 21 or 24 days, respectively	81
	PEG-FeOOH/SiO_2	2−3 nm	nanocomposites became hollow within 24 h and eventually collapsed in FBS	82
	Gold/iron oxide heterostructures	13.4 nm	in citrate medium (pH 4.7): iron oxide shell quickly degraded within several hours; *in vivo*: degradation process of iron oxide shell last for several months	83
Redox	BSA-NiP NP	105 nm	completely degraded in PBS for 54 h	35
	VS_2@lipid-PEG	35 nm	completely degraded in aqueous solution after 30 days under ambient condition	70
	PEG-MoS_2	105 nm	nearly completely degraded within 7 and 14 days after incubated in PBS with pH value of 7.4 and 5.0, respectively	71
	BSA-EDTA-Mn_3O_4	50 nm	quickly degraded within several minutes in ascorbic acid solution	84
	Fe(III)@WS_2−PVP	108 nm	completely degraded within 1 week after incubated in PBS or citrate medium	85
Enzymolysis	carboxylated SWCNT	/	partially degraded within 24 h with the assistance of MPO, H_2O_2, and NaBr	86
	carboxylated MWCNT	/	nearly completely degraded after incubated in HRP and H_2O_2 for 60 days	87

[a]Abbreviations listed in alphabetical order: BLM, Bleomycin-A5; BSA, bovine serum albumin; DOX, doxorubicin; EDTA, ethylenediaminetetraacetic acid; LPSiNPs, luminescent porous silicon nanoparticles; MWCNT, multiwalled carbon nanotubes; NP, nanoparticles; PBS, phosphate buffer saline; PEG, poly(ethylene glycol); PVP, polyvinyl pyrrolidone; SWCNT, single-walled carbon nanotubes.

phosphide/telluride nanoparticles),[29,33−39] organic nanoparticles (e.g., polymeric nanoparticles and the aforementioned liposomes and albumin),[40−43] and inorganic/organic hybrid nanoparticles (e.g., coordination polymer nanoparticles).[44,45] Among these types, inorganic nanoparticles face greater challenges on the way to clinical translation than organic or inorganic/organic hybrid ones, since the relatively higher stability may contribute greater uncertainties *in vivo* with long-term side effects in some cases.[46,47] In addition, the large-scale preparation of inorganic nanoparticles with good repeatability and homogeneity remains more difficult, especially for certain complex inorganic nanoplatforms. Nevertheless, they are still attracting wide attention due to their additional excellent advantages in function and physicochemical properties (e.g., optical, magnetic, and catalytic performance), which greatly facilitates clinical diagnosis and therapy.[48−51] In the past few years, a couple of reviews have discussed the design, construction, and application of degradable inorganic nanoparticles and placed great expectation on their future development.[26,31,32,51−59] However, most of them focused on one or two types of inorganic nanomaterial. Additionally, besides the function and performance, degradation kinetics is also a very important factor needing to be comprehensively discussed, as it may set obstacles impeding potential clinical translation of the nanoagents. This Review summarizes recent advances in biodegradable inorganic nanoparticles for tumor imaging and treatment, with highlights on degradation behavior both *in vitro* and *in vivo*.

2. DEGRADATION MECHANISM OF INORGANIC NANOPARTICLES

The biodegradability of nanomaterials tremendously affects their biosafety in biomedical applications through reacting with living system via chemical/enzymatic reaction to decompose into tiny fragments favoring discharging from the body or recycling in biological systems.[60] To date, biodegradable inorganic nanoparticles such as silica nanoparticles,[61−63] iron oxide nanoparticles,[64−67] manganese oxide nanoparticles,[15,68,69] transition metal dichalcogenide nanoparticles,[38,70,71] and carbon nanomaterials[72−74] have been widely employed for biomedical applications. According to the triggering factors, the degradation mechanisms of inorganic nanoparticles can be divided into four categories: hydrolysis, chelation, redox, and enzymolysis (Table 1 and Figure 1).

2.1. Hydrolysis. Hydrolysis provides an indispensable strategy for the fabrication of biodegradable inorganic nanomaterials. As a reversible process, the nanomaterials can also undergo a hydrolytic process through interacting with water molecules to break down chemical bonds, leading to the continuous collapse of the nanostructure and ultimate degradation. Silica nanoparticles are a typical biodegradable nanomaterial to adopt this mechanism, which undergo the dissociation process as follows: in an aqueous solution, the silicate with a tetrahedral silanol unit is attacked by a nucleophilic group (−OH) to form a pentacoordinate intermediate. The intermediate is unstable and can spontaneously decompose into Si−O and $Si(OH)_4$, which constitute the main degradation products.[52,75,76] In living systems, silica nanoparticles after intravenous administration are prone to accumulate in mononuclear phagocytic system (MPS)-associated organs and degrade into nontoxic products (i.e., $Si(OH)_4$) within a few days.[29] $Si(OH)_4$ naturally exists in many tissues and can also be excreted through renal clearance, showing the promise of silicon-based nanoparticles for clinical translation.[77]

2.2. Chelation. Chelation is another strategy to degrade inorganic nanoparticles, which relies on the external ligands containing one or more chelation groups to coordinate with metal ions originating from nanoparticles, thus forming a stable complex. To ensure biosafety, the metal ions derived from the inorganic nanoparticles must exist in the organism originally or can be excreted after metabolism. Iron-related nanoparticles mainly use this degradation pathway, which utilizes endogenous transferrin in living organism or addition of exogenous

DOI: 10.1021/acs.bioconjchem.9b00699
Bioconjugate Chem. 2020, 31, 315−331

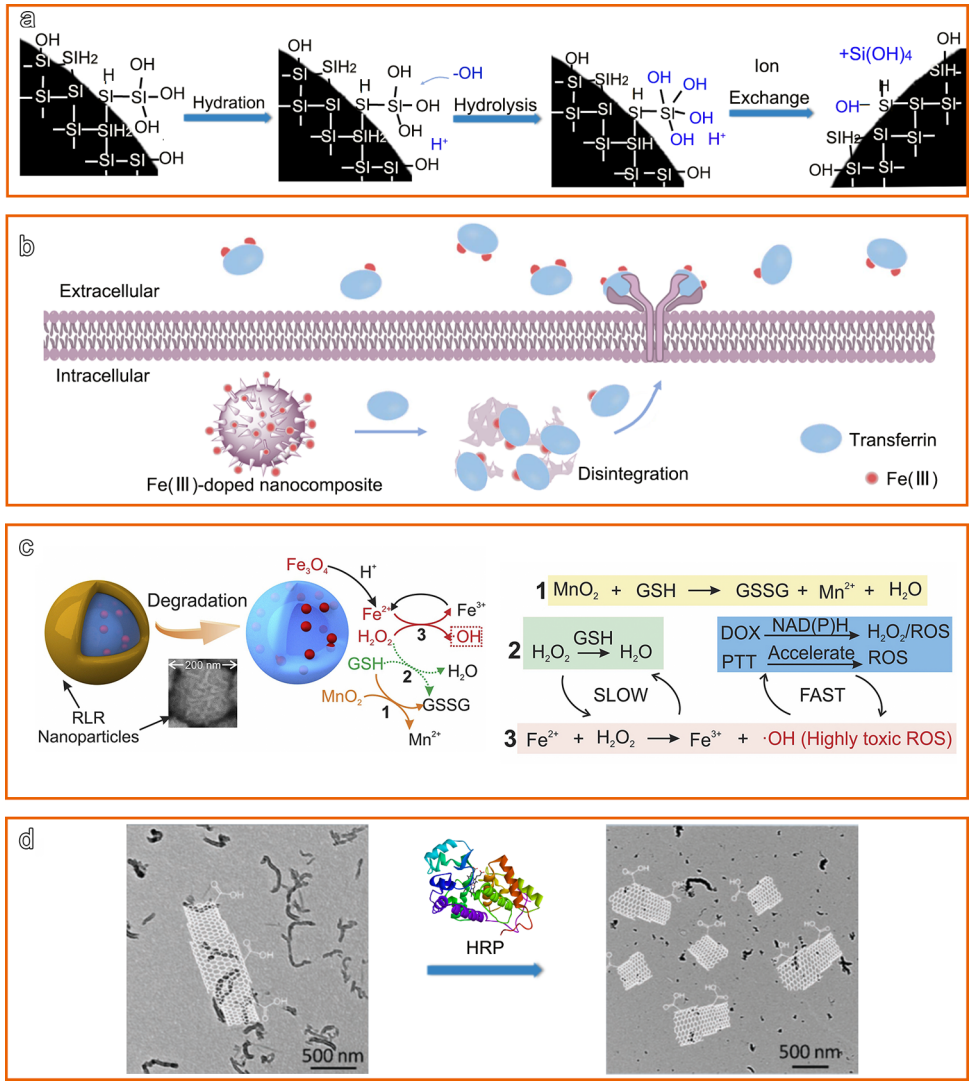

Figure 1. (a) Schematic representation of the degradation process of silicon nanoparticles (reproduced from ref 52 with permission. Copyright 2017, WILEY-VCH Verlag GmbH & Co. KGaA, Weinheim). (b) Chelation and degradation mechanism of iron-containing nanoparticles. (c) Redox degradation mechanism of redox and light-responsive (RLR) nanoparticles (Reproduced from ref 89 with permission. Copyright 2019, Elsevier Ltd). (d) Schematic representation of the enzymatic degradation of multiwalled carbon nanotubes (Reproduced from ref 74 with permission. Copyright 2011, The Royal Society of Chemistry).

ethylenediaminetetraacetic acid (EDTA), desferrioxamine, and deferiprone to chelate, transport, and excrete the excess iron(III).[81,88] For example, due to the high affinity of EDTA, desferrioxamine, and deferiprone for iron(III), iron(III) incorporated in the silica nanoshell could be easily removed by the above chelators, leading to the disintegration of silica nanoshell.[81]

2.3. Redox. The redox strategy generally utilizes reactive oxidative species (ROS) (e.g., hydrogen peroxide, hydroxyl radical) or reducing agents (e.g., glutathione (GSH)) to initiate oxidation or reduction reaction and in-turn breakdown of the matrix, respectively. It is feasible to design inorganic nanoparticles that degrade using redox methodology due to the high efficacy and endogenous availability of redox agents in living systems.[89] Manganese oxide (MnO_2), as a common biodegradable nanoagent, contains Mn−O bond that can specifically dissociate into Mn^{2+} in acidic and reducing environments.[60,90,91] Except for Mn−O, disulfide bonds can be incorporated into inorganic nanoparticles to facilitate the biodegradability due to its easy fragmentation via GSH reduction.[61,92] Moreover, according to the characteristics of oxidants and reducing agents, researchers have constructed a variety of redox-responsive nanoparticles. A degradable WS_2−Fe(III) composite nanoparticle has been found as a self-redox reaction between Fe(III) and WS_2, which leads to biodegradation of WS_2−Fe(III) into soluble Fe(II) and WO_4^{2-}. In addition, the degradation product Fe(II) can further react with H_2O_2 in tumor cells to produce cytotoxic hydroxyl radical (·OH) via the Fenton reaction. Afterward, Fe(II) is oxidized to Fe(III) and further reacted with WS_2 to achieve continuous redox reaction and Fenton reaction.[85]

2.4. Enzymolysis. Enzymes are the basic biocatalysts responsible for biological regulation and metabolism, which can be used to degrade nanoparticles. Enzymatic degradation refers to the interaction of the nanomaterial containing enzyme-sensitive group with corresponding enzyme in the organism, inducing the breakdown of enzyme-sensitive chemical bond and subsequent degradation of the nanoparticle. Once endocytosed by cells, the nanomaterials are always sequestrated and concentrated in lysosomes. The large

DOI: 10.1021/acs.bioconjchem.9b00699
Bioconjugate Chem. 2020, 31, 315−331

Table 2. Represented Inorganic Nanoparticles for Cancer Theranostics[a]

nanoparticle	synthetic method	size	application	ref
PEG-SiO_2/C	hydrolysis	237 nm	PA/drug delivery	14
MnOx-SiO_2	structural difference-based selective etching	100 nm	MRI/drug delivery	68
^{89}Zr-SiO_2 NP	Stöber method	150 nm	PET/drug delivery	94
SiO_2 NP	hydrolysis	3.4 nm	MRI/SDT	79
SiO_2 NP	Stöber method	118 nm	FL imaging	80
SiO_2 NP	Stöber method	180 nm	drug delivery	78
SiO_2 NP	modified surfactant-assembly sol−gel process	150−390 nm	drug delivery	95
Cy7.5-SiO_2	oil−water biphase stratification approach	100 nm	FL imaging	96
PO-PEG iron oxide NP	thermal decomposition	12 nm	T_1-MRI	97
PEG-Fe_3O_4	thermal decomposition	9.8 nm	MRI	98
PEG-Fe_3O_4	thermal decomposition	10.9 nm	MRI	99
PEG-Fe_3O_4	thermal decomposition	22 nm	MRI	100
^{99m}Tc-Fe_3O_4	thermal decomposition	69.2 nm	MRI	101
Cy5.5-Fe_3O_4	thermal decomposition	24 nm	MRI/FL imaging	102
MnO_2	intercalation-deintercalation reaction	200 nm	MRI/drug delivery	69
BSA-EDTA-Mn_3O_4	hydrothermal method	50 nm	MRI/PTT/drug delivery	84
HAS-MnO_2	albumin-based biomineralization method	50 nm	drug delivery	90
Cu_3BiS_3 nanodot	thermal decomposition	21.95 nm	CT/MSOT/PTT/X-ray/IR imaging	31
VS_2@lipid-PEG	thermal decomposition	35 nm	MRI/PA/PTT/SPECT	70
PEG-MoS_2	hydrothermal method	90 nm	PTT	71
Fe(III)@WS_2-PVP	solvothermal method	108 nm	PTT/drug delivery	85
MoS_2	liquid exfoliation	80 nm	FL imaging	96
PEG-$MoTe_2$	chemical vapor transport method	60 nm	PTT/chemotherapy	103
2D boron nanosheet	liquid exfoliation	<100 nm	PA/PTT/FL imaging	104
2D antimonene nanosheet	liquid exfoliation	70 nm	detection	105
2D Ti_3C_2-based MXene nanosheet	selective etching	164 nm	PTT/drug delivery	106
2D SnTe@MnO_2-SP nanosheet	liquid exfoliation	160 nm	PA/PTT	34
BSA-NiP NP	calcine	105 nm	MRI/PA/PTT/CT	35
BP/cellulose hydrogels	liquid exfoliation	5.1−10.8 nm	PTT	107
GO/BPNF aerogel	liquid exfoliation	10−30 nm	PTT	108
PEG-BP	liquid exfoliation	100−200 nm	drug delivery	37
$NaGdF_4$:Ce/Tb@CaP	thermal decomposition	130 nm	MRI/drug delivery	109
CaP	wet-chemical strategy	29.4 nm	drug delivery	110
Sr-CaP	microwave-assisted hydrothermal method	17.2 nm	drug delivery	111
CaP	microwave-assisted solvothermal method	750 nm	drug delivery	112

[a]Abbreviations listed in alphabetical order: BP, black phosphorus; CT, chemotherapy; FL, fluorescence; MSOT, multispectral optoacoustic tomography; GO/BPNF, graphene oxide/black phosphorus nanoflake; PAI, photoacoustic imaging; PDT, photo dynamic therapy; PO, poly(ethylene glycol); PTT, photothermal therapy; 2D, two-dimensional; SDT, sonodynamic therapy; SPECT, single-photon emission computed tomography).

amount of acidic hydrolase residing in the lysosome can degrade the nanoparticles. Carbon nanomaterials are mainly degraded in this way, through enzymatic decomposition by horseradish peroxidase (HRP), myeloperoxidase (MPO), lignin peroxidase (LiP), and manganese peroxidase (MnP) in lysosomes.[67] The degrading efficiency is closely correlated with the structure of nanomaterials. For example, defective sites on the walls and ends of carboxyl-functionalized or nitrogen-doped multiwalled carbon nanotubes (MWCNTs) are more likely to bind to HRP, thus facilitating enzymatic degradation.[87] In addition, some hybrid nanoparticles with organic components can be degraded in this pathway. The dextran-coated iron oxide nanoparticles accumulate in the lysosomal vesicles and are degraded by the lysosomal glucosidase.[64,93] In addition to the lysosomal degradation pathway, studies have shown that a variety of enzymes degrade nanoparticles in the cytoplasm. For example, a tumor-associated enzyme matrix metalloproteinase-2 (MMP-2) can selectively degrade nanoparticles containing an enzyme-cleavable peptide substrate.[86]

3. BIODEGRADABLE INORGANIC NANOPARTICLES

Until now, various kinds of inorganic nanoparticles have been synthesized for biomedical applications, where biodegradable nanoparticles received much attention due to the potentially better biosafety. Table 2 shows some representative inorganic nanoparticles for different cancer theranostics applications.

3.1. Silica Nanoparticles. Silica nanoparticles are the most common biodegradable inorganic nanomaterials, which can degrade into silicic acid or small silica species under specific aqueous media. Due to their widely accepted biocompatibility, they are considered to be one of the most promising platforms for biomedical applications, including imaging diagnosis[29,82,113−115] and drug delivery.[14,61,78,79,116] For instance, Sailor and co-workers prepared luminescent porous silicon nanoparticles by electrochemical etching method. The obtained nanoparticles exhibited near-infrared photoluminescence between 650 and 900 nm under ultraviolet to red excitation and possessed better photostability compared to the common fluorescent dyes, and thus could be used for *in vivo* monitoring and tumor imaging. After being systematically

DOI: 10.1021/acs.bioconjchem.9b00699
Bioconjugate Chem. 2020, 31, 315−331

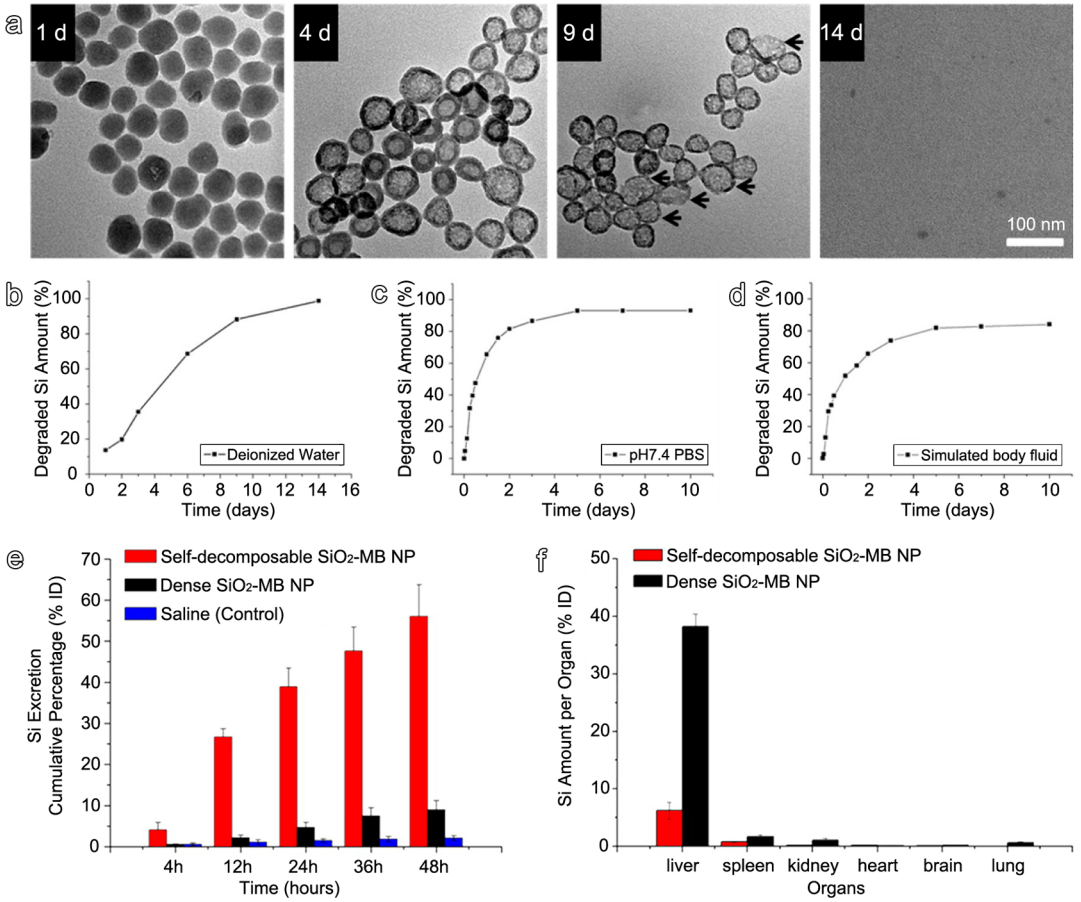

Figure 2. (a) Typical transmission electron microscopy (TEM) images of the SiO_2-methylene blue (MB) NPs after being immersed in deionized water for 1, 4, 9, and 14 days, respectively. (b–d) Inductively coupled plasma optical emission spectrometer (ICP-OES) result of degraded silicon amount as a function of immersion duration in (b) deionized water at room temperature, (c) PBS (pH 7.4), and (d) simulated body fluid (with 50% FBS) at 37 °C. (e) ICP-OES analysis of Si amount in the urine of rats collected at 4 12, 24, 36, and 48 h after injection of self-decomposable, dense SiO_2-MB NPs or saline (as the control). (f) ICP-OES analysis of Si amounts in the organs of rats collected at 48 h after injection of self-decomposable and dense SiO_2-MB NPs. The percentages are calculated by the average amount of Si detected compared to the total injection amount of SiO_2-MB NPs. Data are presented with mean ± SEM, n = 3. (Reproduced from ref 116 with permission. Copyright 2013, American Chemical Society.)

injected into mice, the porous silicon nanoparticles were mainly accumulated in RES such as liver and spleen like many other nanomaterials. However, they could be largely degraded and cleared from the body by renal clearance in 1 week and completely cleared within 4 weeks.[29] Different from the intrinsic luminescence described above, certain fluorescent molecules could be conjugated to the silica nanoparticle surface or incorporated into an inner particle and thus used for *in vivo* tumor diagnosis.[114] Furthermore, other signal units could also be integrated with silica nanoparticles, realizing the corresponding imaging functions, such as magnetic resonance imaging (MRI),[60,79,82] photoacoustic imaging (PAI),[14] and positron emission tomography (PET).[94]

Compared to imaging, silica nanoparticles have received much more attention in drug delivery due to the large specific capacity for drug loading. The loaded drug can be released in a controllable manner with the degradation of silica nanoparticles. Li and co-workers constructed a degradable drug carried system by introducing model drug (e.g., methylene blue (MB), oxazine725, LDS751, and doxorubicin (DOX)) into SiO_2 during the nanoparticle growth under controlled experimental conditions, where the silica precursor (TEOS) and hydrolytic agent (ammonia) concentrations were lower than that for synthesizing dense silica nanoparticles. Under these conditions, a very small amount of silica species was presented and combined with drug molecules to form drug-rich nuclei at the initial stage of synthesis followed by further growth process, resulting in highly concentrated drug in the nanoparticle center and a loose silica network. Systematic investigations showed that the release of drug was primarily driven by diffusion caused by the concentration gradient in silica nanoparticles. With the drug escaping out of the nanoparticles, the silica network began to collapse from the center of the nanoparticle, eventually leading to complete matrix degradation and drug release (Figure 2). The *in vivo* results showed that the amount of degradable silica nanoparticles accumulated in main organs was significantly lower than that of dense silica nanoparticles due to their ease of degradation and subsequent rapid renal excretion.[116] In addition, by further adsorbing model drug onto the drug-encapsulated silica nanoparticle described above, they developed a dual-load drug delivery system. The resulting nanoparticles exhibited a two-phase sustained release with a fast-initial release followed by a long-lasting release pattern, primarily due to different mechanisms, i.e., "weak adsorption" and "relatively strong encapsulation", respectively. The

DOI: 10.1021/acs.bioconjchem.9b00699
Bioconjugate Chem. 2020, 31, 315–331

advantage of dual loading is that the drug release profile can be manipulated on demand by appropriate control of the synthetic conditions, which is very meaningful for the therapy of different diseases.[78] Another way to control drug release is to construct smart degradable silica nanocarriers. For example, by introducing disulfide bond bridged silane in the synthesis, Zhang and co-workers developed a GSH-responsive degradable silica nanoshell for loading DOX. The *in vitro* experimental results demonstrated that the release of DOX significantly depends on GSH. The cumulative release of DOX in the presence of 10 mM GSH was more than twice that in the absence of GSH.[61]

Although the biodegradability of silica nanoparticles has been demonstrated by many researchers, the degradation rate varied significantly for each study. Degradation kinetics is one of the key factors to consider when designing silica nanoparticle-based drugs, not only due to the potential toxicity caused by retention *in vivo*, but also because the release kinetics of drug loaded in the nanoparticles are strongly related to the degradability of silica nanoparticles. To date, the degradation kinetics of silica nanoparticles have been found to depend on many factors, including porous structures, size, surface coating, composition, shape, and the external environment.

Typically, mesoporous silica nanoparticles (MSNs) are more susceptible to degrade both *in vitro* and *in vivo* than the nonporous ones.[116−119] Compared with dense silica nanoparticles that will take several weeks or longer to fully degrade, the porous structure of silica nanoparticles largely increases the degradation rate and the decomposition can be completed in one or several days. In addition, the degradation kinetics can be adjusted by the porous structures. Zhao and co-workers synthesized serious 3D-dendritic MSNs with average pore size varied from 2.8 to 13 nm and found that the degradation rate in simulated body fluid was mainly dependent on the pore size of MSNs.[118] The larger the pore size, the faster the degradation rate. This can be explained by the fact that the larger porous structure can on one hand reduce the cross-linking degree of silica frameworks, and on the other hand accelerate substance diffusion between inside and outside, which will both contribute to the degradation. Due to the well-designed porous structures, the fastest degradation could be completed entirely in 24 h.

Size is another factor that would affect the metabolic behavior of MSNs. However, unlike the porous structure that can largely alter the degradability of MSNs, size has a limited effect on the degradation kinetics *in vitro*. Lu and co-workers prepared different sized (150, 200, 310, 390 nm) MSNs by the Stöber method and then immersed them in simulated body fluid. The degradation curves showed that MSNs with different sizes had almost the same degradability, and over 90% of MSNs degraded after 2 days of incubation, regardless of the particle size.[95] In other research, Kuroda and co-workers synthesized four different-sized MSNs with diameter between 20 and 80 nm and showed similar degradation kinetics in phosphate buffer saline (PBS). However, they found that the dispersity of MSNs had a significant effect on the degradability. After being dried under 120 °C for 24 h, the degradation rate largely decreased due to the aggregation of MSNs.[117] Unlike the *in vitro* behavior, the size of MSNs had an obvious effect on the *in vivo* degradation. To reveal the effect of size on biodistribution and metabolism *in vivo*, Shi and co-workers prepared bare MSNs and poly(ethylene glycol) (PEG) coated MSNs with particle sizes of 80, 120, 200, and 360 nm.[120] After being systematically injected into mice, MSNs with larger particle size showed a faster degradation rate and higher urinary excretion of the degradation products, regardless of the surface modification. This is because larger particles are more easily captured by RES including liver and spleen, resulting in faster degradation and consequently larger excretion. In addition, the surface modification can also alter the biodistribution and metabolism of MSNs *in vivo*. After PEGylation, MSNs can more easily escape from the capture by RES and have a longer blood circulation time. Furthermore, PEGylation can slower down the degradation and excretion of MSNs. Although the authors explained that the decreased degradation was caused by the lower RES capture due to PEGylation, the hindering effect of surface modification on the degradability of MSNs themselves cannot be ignored.[29,121] In a study carried out by Cauda et al., MSNs with different PEG chain length and density were first prepared and then the degradability was investigated in simulated body fluid. Compared to uncoated MSNs, surface PEGylation could significantly reduce the degradation rate, and the longer and denser polymer shells were more efficient in slowing down the degradation kinetics.[121]

The degradability of silica nanoparticles can also be adjusted by metal ion-doping.[60,81,122,123] Generally, the degradability of metal ion-doped silica nanoparticles depends on the stability of the metal−oxygen bond (−M−O−) in the −Si−O−Si− framework of silica nanoparticles. For example, Trogler and co-workers doped iron(III) into silica nanoshell during sol−gel synthesis. The iron incorporation degraded the resultant nanoshell in several days in the presence of chelators, including EDTA, desferrioxamine, and deferiprone. In contrast, no change was observed for the iron(III) doped silica shells incubated in Milli-Q water or PBS. The results indicate that the chelators can remove iron(III) from silica nanoshells and cause matrix decomposition. Further biodegradability testing in mammalian serum containing iron(III) chelating protein transferrin demonstrated the solubilization of iron(III) doped silica nanoshells in fetal bovine serum (FBS) and human serum (HS) after 20−25 days.[81] Compared to the relatively stable −Fe−O− bond, the easily broken −Mn−O− bond makes the Mn-doped silica nanoparticles more susceptible to degradation in the physiological environment. Shi and co-workers constructed Mn-doped MSNs and developed a tumor environmentally sensitive theranostic platform by loading DOX into the Mn-doped MSNs. The doped manganese could be easily extracted from the silica matrix in a mild acidic or reducing environment, thus resulting in fast degradation of Mn-doped MSNs and promoting the release of DOX at the tumor site. In addition, the released Mn^{2+} could significantly enhance the contrast of T_1-weighted MRI, which is efficient for tumor diagnosis.[60] Based on a similar concept, Zhang and co-workers first incorporated hydroxyapatite (HAP) into MSNs, and then loaded DOX into the resultant MSNs/HAP hybrid nanoparticles.[122] The experimental results showed that both the degradability of the resultant nanoparticles and the release of DOX were significantly improved due to the removal of Ca^{2+} under mild acidic condition. However, not all metal ion-doping can enhance the degradability of MSNs. In a study carried out by Shi et al., copper-doped MSNs were synthesized as an immunomodulatory agent for inducing osteogenesis. Differently from the iron-, manganese-, and calcium-doped MSNs, the copper doping could slow down the degradation

DOI: 10.1021/acs.bioconjchem.9b00699
Bioconjugate Chem. 2020, 31, 315−331

rate of MSNs in Tris-HCl buffer when the doping ratio reach 5%.[123] We speculate that this is because the Cu−O bond is more stable than the Si−O bond, resulting in the doping of copper making the MSNs more difficult to degrade.

Apart from the previously mentioned factors, some other parameters will also affect the degradability of silica nanoparticles. For example, Tang and co-workers reported that the shape of MSNs could affect the biodistribution and clearance *in vivo*, where short-rod MSNs had a more rapid clearance rate than long-rod MSNs in both hepatic and renal metabolism.[124] In addition, the concentration of silica nanoparticles also has an influence on the degradation kinetics of MSNs, and higher concentrations will decrease the degradation rate and prolong the degradation process.[62] Furthermore, the calcinated silica nanoparticles often show a remarkably lower degradation rate due to the higher condensation level of −Si−O−Si− network.[62]

3.2. Iron Oxide Nanoparticles. Iron oxide nanoparticles hold great promise in biomedical applications such as MRI contrast agent[30,97−99,125−127] and magnetic hyperthermia.[128−130] Due to the outstanding magnetic properties and biocompatibility, several iron oxide nanoparticle-based drugs have been clinically approved since the 1990s, among which Feridex is the most famous one as a MRI contrast agent. In the past two decades, with the development of synthetic technologies, iron oxide nanoparticles with various sizes,[131−133] morphologies,[100,134] and surface modifications[135,136] have been developed and the performances have also been largely improved to satisfy the different requirements of specific applications. For instance, the relaxivity can be enhanced by increasing the particle size and optimizing the surface modification.[132,135] In addition, iron oxide-based multimodality imaging nanoprobes integrating MRI and other functionalities, such as nuclear imaging,[101,137,138] fluorescence imaging,[102,139] and photoacoustic imaging,[66] can take advantage of each modality and greatly improve the diagnostic accuracy. However, the practical imaging performance is also influenced by the *in vivo* pharmacokinetics. In general, the pharmacokinetics of iron oxide nanoparticles *in vivo* can be affected by many factors, such as size and surface modification. Nanoparticles with smaller size are more likely to escape from the uptake of RES and usually possess longer blood circulation time. In addition, the surface biocompatible polymer coating can enhance the colloidal stability of the underlying nanoparticle and reduce the interaction with protein, thus exhibiting longer blood circulation time than bare nanoparticle. However, most of the nanoparticles eventually accumulate in RES (mainly located in the lysosomes of RES cells), and then partly decompose with the majority transformed to ferritin and/or hemosiderin. Based on this feature, Ferumoxytol (Feraheme), iron oxide nanoparticles coated by polyglucose sorbitol carboxymethyl ether, has been approved by the FDA for treatment of human anemia.

Compared to other inorganic nanoparticles, it is difficult to trace iron oxide nanoparticles in organisms by the gold standard method (i.e., elemental analysis), because the high background of endogenous iron makes it difficult for elemental analysis to quantitatively analyze exogenous nanoparticles. Although the excellent magnetic properties endow iron oxide nanoparticles good relaxation enhancement of surrounding protons that can be followed up by MRI,[140−142] the quantification *in vivo* remains challenging. Radiolabeling provides an alternative way for tracking nanoparticles *in vivo*, while the accuracy largely depends on the stability of the resultant radiolabeled iron oxide nanoparticles.[101,143,144] Most importantly, all these methods can hardly distinguish the degraded nanoparticles from intact ones. To reliably monitor the degradation kinetics of iron oxide nanoparticles, Gazeua and co-workers combined different characterization methods, including ferromagnetic resonance (FMR), superconducting quantum interference device (SQUID) magnetization measurement, elemental analysis, and transmission electron microscopy (TEM), where FMR can quantify the magnetization and distinguish the ferrimagnetic nanoparticles from paramagnetic ion species, magnetization curve profiles can assess the size distribution of nanoparticles, elemental analysis detects the total iron content or iron ion concentration, and TEM gives a visualized variation of iron oxide nanoparticles at the nanoscale.[145] Since iron oxide nanoparticles are usually taken up via endocytosis and trapped in lysosomes, the degradation of iron oxide nanoparticles was first evaluated in citrate buffer to mimic the lysosomal environment. With the incubation time prolonged, the magnetization of iron nanoparticles suspension gradually decreased, while the shape of normalized magnetization curves and field cooled/zero-field cooled (FC/ZFC) curves remained unchanged, indicating the overall size distribution of the remaining nanoparticles was not significantly changed during degradation, which was further confirmed by the FMR measurement and TEM observation. This behavior is totally different from that of silica nanoparticle mentioned above, which usually exhibits synchronous degradation for all individual nanoparticles.

By using the aforementioned complementary techniques, the persistence, biodegradation, and biotransformation of iron oxide nanoparticles *in vivo* can also be evaluated.[146] At each time point, the concentration of nonferromagnetic iron (including endogenous iron and degradation products of iron oxide) can be quantified by comparing the difference between inductively coupled plasma optical emission spectrometer (ICP-OES) results (representing total iron concentration) and FMR results (representing iron concentration in iron oxide nanoparticles). After intravenous injection into mice, the fate of iron oxide nanoparticles was monitored for three months. FMR results indicated that iron oxide nanoparticles were mainly sequestered by liver and spleen at an early time post-injection. Over time, the FMR signal gradually decreased both in liver and in spleen, indicating the degradation and/or elimination of iron oxide nanoparticles. In addition, the nonferromagnetic iron in the spleen gradually increased, while it was almost constant in the liver. The increase of nonferromagnetic iron in spleen was even higher than the iron oxide uptake by spleen at the early time (1 day) post-injection, evidencing a redistribution of degradation products of nanoparticles from the liver to the spleen. Further magnetic properties and morphologies obtained by SQUID and TEM suggested that part of the iron oxide nanoparticles degraded and transformed into poorly or non-magnetic iron (e.g., ferritin and hemosiderin), while the rest of the nanoparticles still retained their initial size distribution and magnetic properties, which was consistent with the *in vitro* degradation behavior.[145] Since the inherent efficacy of iron oxide nanoparticles (e.g., the MR contrast enhancement) depends largely on the sized-related magnetic properties, the preserved size distribution during degradation can help to simplify the interpretation of imaging results over time.

DOI: 10.1021/acs.bioconjchem.9b00699
Bioconjugate Chem. 2020, 31, 315−331

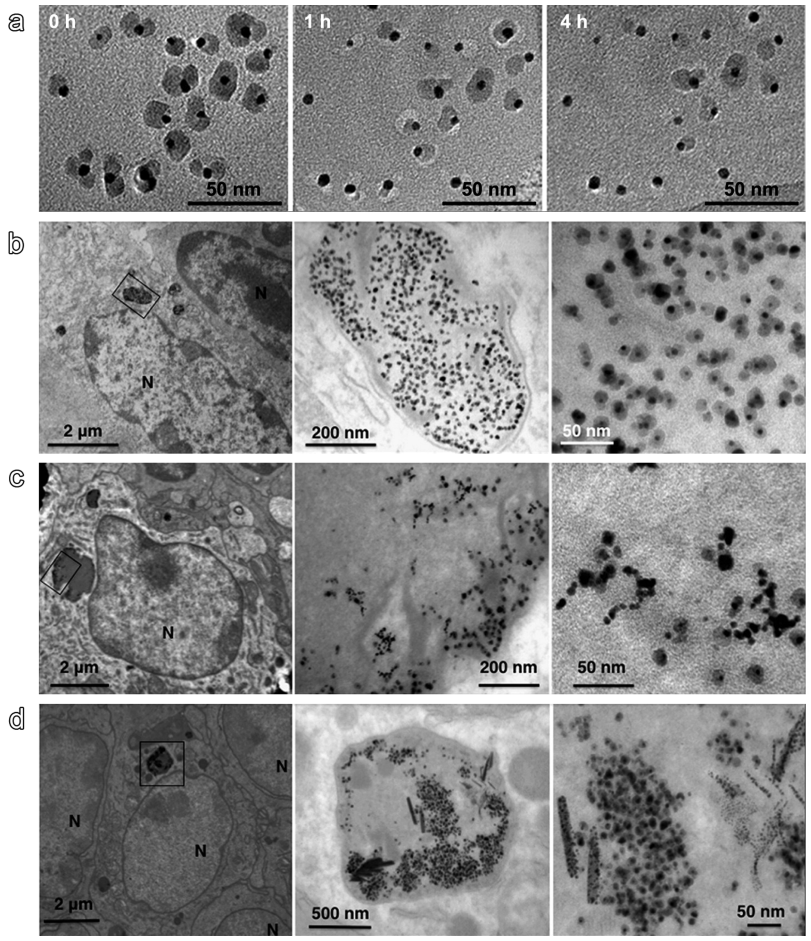

Figure 3. (a) TEM monitoring of single polymer-coated gold/iron oxide nano-heterostructures (NHs) immersed in the acidic medium for 0, 1, and 4 h. We observe the progressive dissolution of iron oxide moieties, leaving resilient gold particles. Note that the dissolution is not homogeneous among NHs. (b) Spleen section at D1 when NHs, localized in splenic lysosomes, do not exhibit any particular alterations (with gradual magnifications of the zone in the square). (c) At D7, gold core residues start forming characteristic chains, which coexist with unaltered heterostructures. (d) Spleen at D90 where distinctive chains and assemblies of gold residues are manifested together with unaltered heterostructures. (Reproduced from ref 83 with permission. Copyright 2015, American Chemical Society.)

To reveal the life cycle of iron oxide nanoparticles in the body, Gazeua and co-workers further constructed a gold/iron oxide heterostructure and systematically investigated their degradability (Figure 3).[83] In comparison with iron oxide, gold is more inert to the external environment and thus can be used as tracers to highlight the local degradation of iron oxide. The *in vitro* TEM results indicated that the resultant nanocomposites exhibited an uneven degradation of iron oxide around gold in the citrate buffer, which was similar with the pure iron oxide nanoparticles.[65] After being intravenously injected into mice, the transformation of nanocomposites in the major organs were tracked by TEM for one year. The injected particles were mainly present in lysosomes of microphage-like cells (e.g., Kupffer cells in liver and macrophages in spleen) regardless of the time point. At day 1 post-injection, the intact nanocomposite was well separated due to the surface polymer protection. From day 7 up to 1 year, with the gradual degradation of iron oxide, nanocomposites tended to form chains, lattices, or clusters, suggesting the polymer shell had been also degraded. In addition, it was surprisingly found that although no degradation was observed *in vitro*, the average diameter of gold cores diminished from the initial 5 to 3 nm at 30 days post-injection, indicating gold nanoparticles could also be eroded *in vivo* under the biological effectors of lysosomes.[83] However, some of the nanocomposites still resisted degradation even over 1 year after administration, which was in line with the previous investigations that each individual nanoparticle had different degradation kinetics.[145−147] Although the reason is still unclear, it is apparent that the degradability of iron oxide nanoparticles can be affected by many factors.

First, the degradation of iron oxide nanoparticles strongly depends on the surface modification. For instance, dextran coated nanoparticles are more prone to degradation than the phosphonate glucose coated ones in citrate buffer.[145] The surface modification-dependent degradability can be attributed to the accessibility of iron chelator to the iron oxide core. Surface ligands with higher anchoring stability with iron oxide are more likely to resist the complexation of chelator and reduce the degradation rate. In addition, the PEGylated iron oxide nanoparticles show much higher degradation rate than amphiphilic polymer coated ones both *in vitro* and *in vivo*.[65,83] The hydrophobic layer in the amphiphilic polymer decorated iron oxide nanoparticles can effectively prevent the particle core from contacting the chelator, thus showing higher stability than the hydrophilic PEG coated ones in the simulated intracellular environment. Furthermore, the surface modifica-

DOI: 10.1021/acs.bioconjchem.9b00699
Bioconjugate Chem. 2020, 31, 315−331

tion will also alter the biodistribution of iron oxide nanoparticles and definitely affect the degradation behavior *in vivo*.

Another parameter that can affect the degradation of iron oxide nanoparticles is pH.[64,145] In citrate buffer, the degradation rate of iron oxide nanoparticle is in the order of pH 4 > pH 3 > pH 4.7 > pH 2.4, regardless of type of nanoparticles.[145] The trend of irregular variation can be attributed to the antagonistic effect of the enhanced degradable nature of iron oxide and the decreased chelating ability of citrate with pH value decreasing. Furthermore, it is found that chelator is an indispensable factor for the degradation of iron oxide nanoparticles in simulated physiological media. Iron oxide nanoparticles are not readily soluble in physiological buffers without chelators, regardless of pH.[64]

The ratio between chelator and iron concentration also plays an important role in the degradation of iron oxide nanoparticles. By increasing the ratio of chelator to iron concentration, the degradation kinetics can be greatly accelerated.[83,145] This conclusion can be further demonstrated by the *in situ* observation of the degradation process. When using TEM to monitor the degradation behavior of iron oxide nanocubes *in situ*, a very small amount of nanocubes were first deposited on the carbon-coated TEM grid and then immersed into lysosome-like medium. The deposited iron oxide nanocubes can fully degrade within serval hours due to the large chelator/iron concentration ratio, while this degradation process takes several days to finish in a nanocube suspension.[65] Furthermore, it has also been found that the monolayer nanocubes are more susceptible to degrade than the aggregates, and the periphery of the aggregates degrade more rapidly than the inner part, indicating the aggregation tends to prevent degradation by limiting the accessibility of chelators to nanoparticles.

3.3. Manganese Oxide Nanoparticles. Manganese oxide nanoparticles (usually MnO_2 nanoparticles) are considered to be good platforms for constructing intelligent imaging probes due to their degradability in the tumor microenvironment. MnO_2 nanoparticles are relatively stable under neutral and basic condition, while can be easily decomposed into Mn^{2+} and O_2 at reduced pH. In contrast to MnO_2 nanoparticles that usually have very low relaxivity (r_1 typically less than 1 $mM^{-1}\cdot s^{-1}$), Mn^{2+} ions exhibit an outstanding MRI contrast effect due to its five unpaired 3d electrons. Based on this property, many pH-responsive MRI nanoprobes were constructed and effective cancer diagnoses were achieved.[15,68,69,148] For instance, Wang and co-workers prepared PEGylated-MnO_2 nanosheets via exfoliation using layered Na-MnO_2 as material. Due to the high valence state (IV) of manganese and shielded paramagnetic centers inaccessible to water molecules, the initial nanosheet possessed an extremely low r_1 of 0.007 $mM^{-1}\cdot s^{-1}$. However, after soaking in acidic buffer for 2 h, the r_1 value substantially increased to 3.4 and 4.0 $mM^{-1}\cdot s^{-1}$ at pH 6.0 and 4.6, respectively. To further evaluate the pH-responsiveness *in vivo*, the resultant MnO_2 nanosheets were directly injected into tumor and normal tissue for comparison. The tumor site showed clear positive contrast enhancement, while no significant signal enhancement was observed at the subcutaneous injection site, fully evidencing the degradation of MnO_2 and release of Mn^{2+} under mildly acidic tumor microenvironment.[69] In addition, based on the pH-responsiveness, MnO_2 nanomaterials can also serve as an intelligent drug delivery system.[68,69,148] Certain drugs (e.g., DOX and Ce6) can be loaded onto the surface of MnO_2 nanomaterials via electrostatic interaction, coordinate bonding, and covalent coupling. The loaded cargos can be simultaneously released at the tumor site when the nanoparticles break down, thus enabling the on-demand drug delivery.

Apart from the pH-triggered degradation, MnO_2 nanoparticles also present redox-responsive property, which makes them subject to the reduction of Mn(IV) into Mn(II). For example, it can be reduced by GSH that is abundant in tumor, leading to the disintegration of MnO_2. Using this feature, Tan and co-workers designed a smart MnO_2-based nanosystem for enhanced photodynamic therapy (PDT), where the photosensitizer Ce6 was adsorbed on the MnO_2 nanosheets. On one hand, MnO_2 nanosheets can enhance the cellular uptake of photosensitizers and inhibit the extracellular singlet oxygen ($^1O_2$) generated by Ce6, which may lead to side effects. On the other hand, MnO_2 nanosheet can react with intracellular GSH, resulting in the degradation of nanosheets, thus releasing Ce6 for photodynamic therapy. Furthermore, the reaction between MnO_2 and GSH will deplete the intracellular GSH, thereby reducing its scavenging effect on $^1O_2$ and eventually enhancing the PDT efficiency.[149] Besides endogenous GSH, the artificially introduced reductant (e.g., ascorbic acid) can also motivate the degradation of MnO_2 both *in vitro* and *in vivo*.[84]

Although many studies have shown that the degradation products, i.e., Mn^{2+}, can be excreted by renal clearance,[15,148] the elimination amount is not clear and we still cannot rule out the retention of manganese ions in the body. As previously demonstrated, the toxicity of Mn^{2+} is much higher than that of manganese oxide nanoparticles. To address this problem, Zhou and co-workers developed a degradable EDTA and BSA-capped Mn_3O_4 nanoparticles. The obtained nanoparticles showed strong adsorption in the near-infrared (NIR) region and a photothermal conversion efficiency of 34.7% under 785 nm, and thus could be potentially used for photothermal therapy. After being intravenously injected into tumor-bearing mice, the constructed nanoprobes could accumulate at the tumor site and then accelerate degradation with the assistance of artificially introduced ascorbic acid, enabling the MRI-guided phototherapy. Most importantly, the released Mn^{2+} could be captured by the surface loaded EDTA, thus accelerating the excretion and decreasing the potential toxicity.[84]

Compared to iron oxide nanoparticles, manganese oxide nanoparticles are more susceptible to degradation under physiological conditions. In a previous study reported by Wang and co-workers, iron oxide nanoparticles were first incorporated into a chitosan-based nanocluster, and subsequently manganese oxide nanoparticles were loaded onto the nanocluster surface to form an iron oxide/manganese oxide coloaded hybrid nanogel.[150] Due to the strong interference of manganese species, the transverse relaxivity (r_2) of iron oxide nanoparticles was severely reduced (45.7 $mM^{-1}\cdot s^{-1}$ vs 362 $mM^{-1}\cdot s^{-1}$). The resultant nanogel was relative stable under neutral condition, but Mn ions gradually leached out when treated by acidic buffer, resulting in largely recovered r_2 (i.e., 226 $mM^{-1}\cdot s^{-1}$ after being incubated in pH = 5.5 PBS for 3 h). In addition, the released Mn ions also leaded to a much higher longitudinal relaxivity (from 8.9 $mM^{-1}\cdot s^{-1}$ to 15.3 $mM^{-1}\cdot s^{-1}$). The "turn on" effect of both T_1 and T_2 relaxation under acidic condition enabled the resultant hybrid nanogel a highly efficient and specific contrast agent for T_1/T_2 dual-mode MRI tumor diagnosis. The results also suggested that manganese oxide was more degradable than iron oxide,

DOI: 10.1021/acs.bioconjchem.9b00699
Bioconjugate Chem. 2020, 31, 315−331

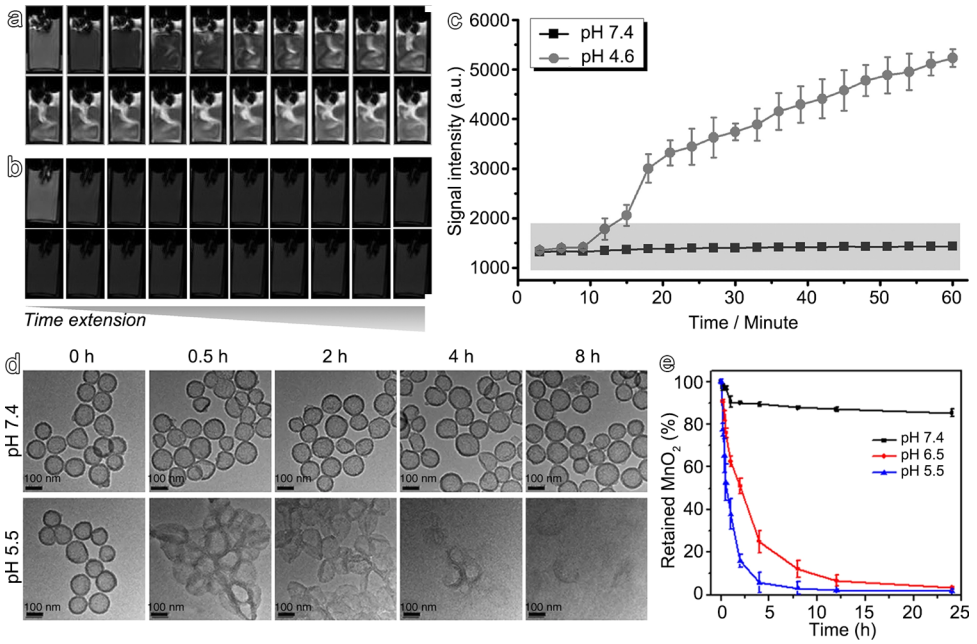

Figure 4. *In vitro* dynamic measurement of T_1-MRI of PEG-MnO_2 in either mildly acidic environment (pH = 4.6, a) or neutral conditions (pH = 7.4, b). (c) T_1-MRI signal intensities of PEG-MnO_2 aqueous solutions under pH 7.4 and 4.6 for prolonged periods. The T_1-MRI images were obtained every 3 min after soaking PEG-MnO_2 nanosheets in the buffer solution at various pH values. (Reproduced from ref 69 with permission. Copyright 2014, WILEY-VCH Verlag GmbH & Co. KGaA, Weinheim.) (d) TEM images of hollow mesoporous MnO_2-PEG (H-MnO_2-PEG) after incubation in buffers with different pH (7.4 and 5.5) for various periods of time. (e) Degradation behavior of H-MnO_2-PEG dispersed in different pH (7.4, 6.5, and 5.5) determined by the absorbance of MnO_2. (Reproduced from ref 148 with permission. Copyright 2017, Springer Nature.)

which may correlate with the solubility product of the corresponding metal hydroxide.

Generally, manganese oxide nanomaterials can degrade within a few hours in the proper physiological environment. Due to the greatly improved MRI contrast enhancement after decomposition, degradation process of MnO_2 nanosheet can be monitored by MRI. As shown in Figure 4a–c, the obtained nanosheets enabled substantial T_1 MRI signal enhancement after being immersed in pH 4.6 buffer for 1 h, while negligible signal change was observed in neutral buffer (pH 7.4).[69] Since the degradation of manganese oxide nanoparticles is very sensitive to the acidic condition, the degradation kinetics can be easily adjusted by controlling the pH of external environment. As given in Figure 4d,e, when the pH changed from 7.4 to 5.5, the degradation of MnO_2 nanoshell could be greatly accelerated. In addition, since the loaded drugs could be synchronously released along with the decomposition of manganese oxide nanoparticles, the on-demand release of drug could also be achieved.[148]

3.4. Transition Metal Dichalcogenide Nanoparticles. Transition metal dichalcogenide nanoparticles (TMDCs), emerging as a class of key materials in chemistry and electronics due to their intriguing chemical and electronic properties, are generally described as the formula of MX_2, where M is the transition metal typically from groups 4–7 of the periodic table (e.g., Mo, W, Ti, V) and X is chalcogen such as S, Se, or Te.[151] In recent years, TMDCs have attracted great interest for phototherapy and drug delivery due to the excellent photothermal effect aroused by unique optical properties and the extraordinary specific surface area enabled by the two-dimensional structures.[70,71,96,103] While the transition metals evolved in TMDCs provoked particular concerns about the risk of toxicity, the rapid elimination of TMDCs from the body becomes a key factor that would affect their further application in biomedicine.

To study the biodistribution, excretion, and toxicology profiles of TMDCs, Liu and co-workers systematically investigated the *in vitro* and *in vivo* behavior of three types of PEGylated TMDCs, including molybdenum dichalcogenides (MoS_2), tungsten dichalcogenides (WS_2), and titanium dichalcogenides (TiS_2) nanosheets (Figure 5).[38] After being intravenously injected into mice, most of the nanosheets accumulated in the RES organs. After 30 days, MoS_2-PEG could be almost excreted through both renal and fecal pathways, while large amounts of WS_2-PEG and TiS_2-PEG were still retained in the body. To unclose the mechanism of different metabolic behavior, PEGylated TMDCs were dispersed in PBS at room temperature and monitored for three months. The variation in absorbance exhibited significant differences in the long-term incubation, where WS_2-PEG showed only a slight decrease, while both MoS_2-PEG and TiS_2-PEG decreased remarkably. However, different from the colorless solution left for MoS_2-PEG, white TiO_2 precipitate was observed in the TiS_2-PEG sample. Further X-ray photoelectron spectroscopy (XPS) demonstrated that most of the $Mo^{IV}S_2$ nanosheets were oxidized to $Mo^{VI}O_4^{2-}$ after three-month storage in PBS. Due to the better chemical stability of W^{IV} and stronger chemical bond of W–S, only a part of W^{VI} was observed in the WS_2-PEG sample, indicating the formation of $W^{IV}S_2/W^{VI}O_3$ compounds after incomplete oxidation. Based on the above results, the following different mechanisms for *in vivo* behaviors of the three types of TMDCs were concluded. Due to the distinctive chemical properties, WS_2 possesses relatively high stability and is hardly degraded in the physiological environment, thus retaining in RES organs for a long time; TiS_2 is unstable and can be gradually transformed into water-insoluble TiO_2 aggregates that cannot

DOI: 10.1021/acs.bioconjchem.9b00699
Bioconjugate Chem. 2020, 31, 315–331

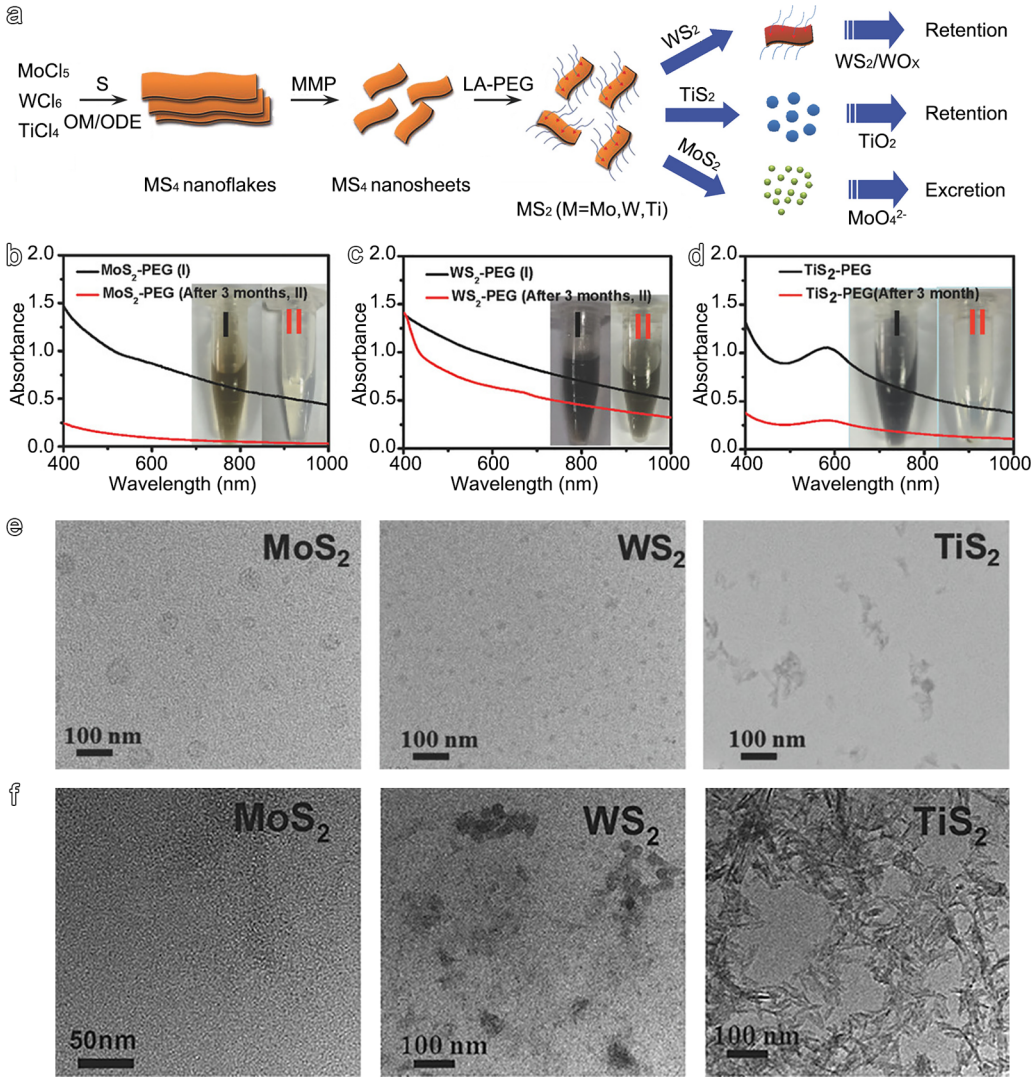

Figure 5. (a) Scheme of transition metal dichalcogenide MS_2-PEG (M = Mo, W, Ti) nanosheet synthesis process and the different pathways of the clearance of MS_2-PEG nanosheets. (b–d) UV–vis-NIR spectra of MS_2-PEG (I) before and (II) after three months standing in PBS at the concentration of 0.02 mg/mL, (b) MoS_2-PEG, (c) WS_2-PEG, and (d) TiS_2-PEG. Inset: Photos of the MS_2-PEG samples before (I) and after (II) three months standing in PBS solution. (e,f) TEM images of PEGylated MoS_2, WS_2, and TiS_2 nanosheets (e) before and (f) after three months standing. (Reproduced from ref 38 with permission. Copyright 2016, WILEY-VCH Verlag GmbH & Co. KGaA, Weinheim.)

be easily eliminated from the body; MoS_2, in marked contrast, can be oxidized and transformed into water-soluble MoO_4^{2-} species in physiological environment, allowing ready excretion via both renal and fecal pathways. Given all this, MoS_2 may be more promising for further biomedical applications due to its biodegradability and relatively rapid excretion. Through the similar degradation mechanism of MoS_2, VS_2 nanodots are also found to be gradually oxidized and degraded into water-soluble V^V-oxide small molecular species (e.g., VO_4^{3-}, $V_2O_7^{4-}$, and VO_3^-), and hence be effectively excreted without appreciable toxicity. Therefore, integrating the intrinsic paramagnetism with strong NIR absorbance as well as chelator-free radiolabeling ability, VS_2 has successfully served as a good nanoplatform for MR/PA/single photon emission computed tomography (SPECT) trimodal imaging guided photothermal cancer therapy.[70]

Similar to the aforementioned nanomaterials, the degradation of TMDCs also depends on the external environment. As noted above, degradation of TMDCs is often associated with the oxidation of transition metals, and therefore, oxidants undoubtedly have a significant impact on the degradation kinetics. Zhao and co-workers systematically evaluated the translocation, biotransformation-related degradation, and toxicity of polyvinylpyrrolidone-modified MoS_2 nanosheets, and found that the biodegradability in biomicroenvironments are in the order of H_2O_2 < catalase < myeloperoxidase, with typical physiological concentrations.[96] Additionally, the degradation rate of MoS_2 under various pH conditions is also distinctly different. The rapid degradation of MoS_2 was observed in neutral pH solution, while degradation was much slower under the weakly acidic condition simulating the tumor microenvironment.[71] Furthermore, the external stimulation such as NIR irradiation would also accelerate the degradation of $MoTe_2$ nanosheets.[103]

3.5. Carbon Nanomaterials. Carbon nanomaterials, in particular, carbon nanotubes and graphene, have gathered increasing attention in drug delivery and bioimaging.[152,153] In the early stage, carbon nanomaterials were assumed to be inert to the biological systems due to their rigid and robust structures, and thus were expected to be highly persistent in

DOI: 10.1021/acs.bioconjchem.9b00699
Bioconjugate Chem. 2020, 31, 315–331

organs and tissues. It has been found that the persistence of single-walled carbon nanotubes (SWNTs) in the biological systems can induce obvious toxicities, including oxidative stress, inflammatory response, and pathogenicity.[72,154,155] Nevertheless, recent studies showed that oxidative enzymes derived from the organism may be capable of degrading functionalized carbon nanomaterials. For example, Star and co-workers reported that the carboxylated SWNTs could be degraded under the catalysis of horseradish peroxide in the presence of H_2O_2, whereas nonfunctionalized SWNTs showed insignificant change under the same condition.[73,156] Similar degradability behavior was also observed for graphene oxide when using human neutrophils-derived myeloperoxidase as enzyme.[157] Additionally, it was found that the degradability of graphene oxide was largely dependent on the oxidation degree of the graphene crystal lattice. On one hand, higher oxidation would result in a higher percentage of carboxyl groups on the surface, leading to better colloidal stability given by the increased negative surface charge, which could avoid aggregation and increase the interaction chance between graphene and myeloperoxidase. On the other hand, the positively charged amino acid residues of myeloperoxidase could bind more strongly to the negatively charged surface, thereby enhancing the degradation capability.[157] The enhanced biodegradability would undoubtedly promote the biomedical applications of carbon nanomaterials *in vivo*.[17]

3.6. Other Inorganic Nanoparticles. In addition to the previously mentioned nanomaterials, biodegradability is also found for some other inorganic nanomaterials, such as calcium phosphate (CaP),[112,158] calcium carbonate,[19,159,160] black phosphorus (BP),[33,55,161] transition metal carbides,[162] nitrides and carbonitrides,[163] and layered double hydroxide nanoparticles,[51] which have been investigated for cancer theranostics. CaP, which has similar components to human bone, belongs to ceramic inorganic materials and has good biocompatibility and biological activity.[110,158,164] With porous structure and large specific surface area, CaP nanoparticles could be degraded into Ca^{2+} and PO_4^{3-} required by the human body *in vivo*.[112,165,166] However, the special surface properties and high reactivity of CaP nanoparticles also lead to a series of complex reactions in cells, which may cause apoptosis and necrosis. To reduce the reactivity, Zhu and co-workers designed a Eu^{3+}-doped CaP mesoporous microsphere. Compared with the undoped ones, the Eu^{3+}-doped CaP mesoporous microspheres are more stable with a slower drug release rate, which is beneficial to tumor treatment and can avoid toxicity problems caused by increased calcium ion concentration.[167] BP nanomaterial can also be easily degraded both *in vitro* and *in vivo* due to its inherent susceptibility to oxidation. It has been explored as a photothermal/photodynamic therapy agent due to the wide range of light absorption, high photothermal conversion efficiency, and high singlet oxygen yield under near-infrared laser irradiation.[37,55,108,168] However, due to the easy degradation caused by oxidation, the BP nanoparticles show unstable and short-term photothermal effects.[107,161] To overcome this problem, PEGylation was adopted to improve the physiological stability of BP nanodots in biological applications.[168] Moreover, the BP nanosheets modified with cellulose was also found to have excellent photothermal response and enhanced stability.[107]

4. CONCLUSION AND OUTLOOK

Inorganic nanoparticles have been widely used in the diagnosis and therapy of cancer, while the biopersistence is currently considered to be a key issue hindering their further clinical translation. Biodegradable inorganic nanoparticles that can decompose *in vivo* accelerate the excretion and largely improve the biosafety. In this Review, the theranostic applications of biodegradable inorganic nanoparticles as well as their degradation behaviors are explored. Although great progress has been made in the effective excretion of inorganic nanoparticles by adjusting the biodegradability, many concerns still remain when translating them from the bench to the clinic. First, not only does the accumulation of original inorganic nanoparticles in the body cause harmful side effects, the degradation products may also provoke adverse responses, which need to be systematically evaluated. From this point of view, inorganic nanoparticle such as iron oxide nanoparticles hold greater promise for future clinical translation as the degradation products are the essential elements in human body. Furthermore, inorganic nanoparticles (e.g., silica nanoparticles) with fast degradation kinetics and easily excreted degradation products also have more chances for further translation. Second, the degradation process and metabolic pathways should be clearly investigated to help assess the biosafety and the possible side effects of inorganic nanoparticles, especially when the degradation products cannot be utilized by the organism. Third, it should be noted that degradable nanoparticles are still largely captured by RES. Compared with small molecular probes that can be quickly eliminated from the body,[169,170] the drugs loaded in inorganic nanoparticles would largely accumulate in the RES organs and eventually be released with the nanoparticles decomposing, leading to unexpected toxicities. Finally, to achieve optimal efficacy and biosafety, the degradation kinetics *in vivo* are needed to be adjusted to suit a specific theranostic application. Therefore, the influences of different factors on the degradation behavior, especially the *in vivo* degradation kinetics, of different inorganic nanomaterials need to be investigated in depth. Overall, a great deal of work is still needed to remove the obstacles hindering the clinical applications of inorganic nanoparticles. Nevertheless, we believe that biodegradable inorganic nanoparticles have a strong chance of revolutionizing future cancer diagnosis and therapy.

AUTHOR INFORMATION

Corresponding Author

*E-mail: jfzeng@suda.edu.cn.

ORCID

Jianfeng Zeng: 0000-0001-7654-8724

Mingyuan Gao: 0000-0002-7360-3684

Author Contributions

#H. Z. and J. G. contributed equally to this work.

Notes

The authors declare no competing financial interest.

ACKNOWLEDGMENTS

The authors thank the financial support from the National Key Research and Development Program of China (2018YFA0208800), National Natural Science Foundation of China (NSFC) (81530057, 81720108024, 81771902,

DOI: 10.1021/acs.bioconjchem.9b00699
Bioconjugate Chem. 2020, 31, 315−331

81671754, 81671755, 21503141, 81901803, 81801751), Jiangsu Specially Appointed Professorship, Natural Science Foundation of Jiangsu Province (BK20191418, BK20190811), and Priority Academic Program Development of Jiangsu Higher Education Institutions (PAPD).

REFERENCES

(1) Zhao, N. N., Yan, L. M., Zhao, X. Y., Chen, X. Y., Li, A. H., Zheng, D., Zhou, X., Dai, X. G., and Xu, F. J. (2019) Versatile types of organic/inorganic nanohybrids: From strategic design to biomedical applications. *Chem. Rev. 119*, 1666−1762.

(2) Liu, J., Bu, W., and Shi, J. (2017) Chemical design and synthesis of functionalized probes for imaging and treating tumor hypoxia. *Chem. Rev. 117*, 6160−6224.

(3) Lee, H., Shin, T. H., Cheon, J., and Weissleder, R. (2015) Recent developments in magnetic diagnostic systems. *Chem. Rev. 115*, 10690−10724.

(4) Lee, D. E., Koo, H., Sun, I. C., Ryu, J. H., Kim, K., and Kwon, I. C. (2012) Multifunctional nanoparticles for multimodal imaging and theragnosis. *Chem. Soc. Rev. 41*, 2656−2672.

(5) Shin, T., Choi, Y., Kim, S., and Cheon, J. (2015) Recent advances in magnetic nanoparticle-based multi-modal imaging. *Chem. Soc. Rev. 44*, 4501−4516.

(6) Louie, A. Y. (2010) Multimodality imaging probes: Design and challenges. *Chem. Rev. 110*, 3146−3195.

(7) Barenholz, Y. (2012) Doxil(R) - The first FDA-approved nano-drug: Lessons learned. *J. Controlled Release 160*, 117−134.

(8) Green, M. R., Manikhas, G. M., Orlov, S., Afanasyev, B., Makhson, A. M., Bhar, P., and Hawkins, M. J. (2006) Abraxane(R), a novel Cremophor(R)-free, albumin-bound particle form of paclitaxel for the treatment Of advanced non-small-cell lung cancer. *Ann. Oncol. 17*, 1263−1268.

(9) Almeida, J. P. M., Chen, A. L., Foster, A., and Drezek, R. (2011) *In vivo* biodistribution of nanoparticles. *Nanomedicine 6*, 815−835.

(10) Bourquin, J., Milosevic, A., Hauser, D., Lehner, R., Blank, F., Petri-Fink, A., and Rothen-Rutishauser, B. (2018) Biodistribution, clearance, and long-term fate of clinically relevant nanomaterials. *Adv. Mater. 30*, 1704307.

(11) Arami, H., Khandhar, A., Liggitt, D., and Krishnan, K. M. (2015) *In vivo* delivery, pharmacokinetics, biodistribution and toxicity of iron oxide nanoparticles. *Chem. Soc. Rev. 44*, 8576−8607.

(12) Li, S. D., and Huang, L. (2008) Pharmacokinetics and biodistribution of nanoparticles. *Mol. Pharmaceutics 5*, 496−504.

(13) Soo Choi, H., Liu, W., Misra, P., Tanaka, E., Zimmer, J. P., Itty Ipe, B., Bawendi, M. G., and Frangioni, J. V. (2007) Renal clearance of quantum dots. *Nat. Biotechnol. 25*, 1165−1170.

(14) Zhang, J., Zhang, J., Li, W., Chen, R., Zhang, Z., Zhang, W., Tang, Y., Chen, X., Liu, G., and Lee, C.-S. (2017) Degradable hollow mesoporous silicon/carbon nanoparticles for photoacoustic imaging-guided highly effective chemo-thermal tumor therapy *in vitro* and *in vivo*. *Theranostics 7*, 3007−3020.

(15) Zhu, W. W., Dong, Z. L., Fu, T. T., Liu, J. J., Chen, Q., Li, Y. G., Zhu, R., Xu, L. G., and Liu, Z. (2016) Modulation of hypoxia in solid tumor microenvironment with MnO_2 nanoparticles to enhance photodynamic therapy. *Adv. Funct. Mater. 26*, 5490−5498.

(16) Zheng, X., Ge, J., Wu, J., Liu, W., Guo, L., Jia, Q., Ding, Y., Zhang, H., and Wang, P. (2018) Biodegradable hypocrellin derivative nanovesicle as a near-infrared light-driven theranostic for dually photoactive cancer imaging and therapy. *Biomaterials 185*, 133−141.

(17) Lee, C., Kwon, W., Beack, S., Lee, D., Park, Y., Kim, H., Hahn, S. K., Rhee, S. W., and Kim, C. (2016) Biodegradable nitrogen-doped carbon nanodots for non-invasive photoacoustic imaging and photothermal therapy. *Theranostics 6*, 2196−2208.

(18) Ye, Z., Wu, X., Tan, M., Jesberger, J., Grisworld, M., and Lu, Z. (2013) Synthesis and evaluation of a polydisulfide with Gd-DOTA monoamide side chains as a biodegradable macromolecular contrast agent for MR blood pool imaging. *Contrast Media Mol. Imaging 8*, 220−228.

(19) Zhao, Y., Luo, Z., Li, M., Qu, Q., Ma, X., Yu, S. H., and Zhao, Y. (2015) A preloaded amorphous calcium carbonate/doxorubicin@silica nanoreactor for pH-responsive delivery of an anticancer drug. *Angew. Chem., Int. Ed. 54*, 919−922.

(20) Zong, Y., Guo, J., Ke, T., Mohs, A. M., Parker, D. L., and Lu, Z. R. (2006) Effect of size and charge on pharmacokinetics and *in vivo* MRI contrast enhancement of biodegradable polydisulfide Gd(III) complexes. *J. Controlled Release 112*, 350−356.

(21) Ge, J., Zhang, Q., Zeng, J., Gu, Z., and Gao, M. (2020) Radiolabeling nanomaterials for multimodality imaging: New insights into nuclear medicine and cancer diagnosis. *Biomaterials 228*, 119553.

(22) Liu, J., Yu, M., Zhou, C., Yang, S., Ning, X., and Zheng, J. (2013) Passive tumor targeting of renal-clearable luminescent gold nanoparticles: Long tumor retention and fast normal tissue clearance. *J. Am. Chem. Soc. 135*, 4978−4981.

(23) Yu, M., and Zheng, J. (2015) Clearance pathways and tumor targeting of imaging nanoparticles. *ACS Nano 9*, 6655−6674.

(24) Peng, C., Xu, J., Yu, M., Ning, X., Huang, Y., Du, B., Hernandez, E., Kapur, P., Hsieh, J. T., and Zheng, J. (2019) Tuning the *in vivo* transport of anticancer drugs using renal-clearable gold nanoparticles. *Angew. Chem., Int. Ed. 58*, 8479−8483.

(25) Wei, R., Cai, Z., Ren, B. W., Li, A., Lin, H., Zhang, K., Chen, H., Shan, H., Ai, H., and Gao, J. (2018) Biodegradable and renal-clearable hollow porous iron oxide nanoboxes for *in vivo* imaging. *Chem. Mater. 30*, 7950−7961.

(26) Ehlerding, E. B., Chen, F., and Cai, W. (2016) Biodegradable and renal clearable inorganic nanoparticles. *Adv. Sci. 3*, 1500223.

(27) Zheng, J., Yu, M., and Yu, J. (2019) Renal clearable luminescent gold nanoparticles: From bench to clinics. *Angew. Chem., Int. Ed. 58*, 4112−4128.

(28) Liu, J., Yu, M., Zhou, C., and Zheng, J. (2013) Renal clearable inorganic nanoparticles: A new frontier of bionanotechnology. *Mater. Today 16*, 477−486.

(29) Park, J. H., Gu, L., von Maltzahn, G., Ruoslahti, E., Bhatia, S. N., and Sailor, M. J. (2009) Biodegradable luminescent porous silicon nanoparticles for *in vivo* applications. *Nat. Mater. 8*, 331−336.

(30) Qiao, R. R., Yang, C. H., and Gao, M. Y. (2009) Superparamagnetic iron oxide nanoparticles: From preparations to *in vivo* MRI applications. *J. Mater. Chem. 19*, 6274−6293.

(31) Liu, J., Wang, P., Zhang, X., Wang, L., Wang, D., Gu, Z., Tang, J., Guo, M., Cao, M., Zhou, H., et al. (2016) Rapid degradation and high renal clearance of Cu_3BiS_3 nanodots for efficient cancer diagnosis and photothermal therapy *in vivo*. *ACS Nano 10*, 4587−4598.

(32) Yang, G., Phua, S. Z. F., Bindra, A. K., and Zhao, Y. (2019) Degradability and clearance of inorganic nanoparticles for biomedical applications. *Adv. Mater. 31*, 1805730.

(33) Shao, J. d., Xie, H. h., Huang, H., Li, Z. b., Sun, Z. b., Xu, Y. h., Xiao, Q. l., Yu, X. F., Zhao, Y. t., Zhang, H., et al. (2016) Biodegradable black phosphorus-based nanospheres for *in vivo* photothermal cancer therapy. *Nat. Commun. 7*, 12967.

(34) Zhang, H., Zeng, W., Pan, C., Feng, L., Ou, M., Zeng, X., Liang, X., Wu, M., Ji, X., and Mei, L. (2019) SnTe@MnO_2-SP nanosheet-based intelligent nanoplatform for second near-onfrared light-mediated cancer theranostics. *Adv. Funct. Mater. 29*, 1903791.

(35) Liu, Y., Zhen, W., Wang, Y., Liu, J., Jin, L., Zhang, T., Zhang, S., Zhao, Y., Yin, N., Niu, R., et al. (2019) Double switch biodegradable porous hollow trinickel monophosphide nanospheres for multimodal imaging guided photothermal therapy. *Nano Lett. 19*, 5093−5101.

(36) Cao, Z., Zhang, L., Liang, K., Cheong, S., Boyer, C., Gooding, J. J., Chen, Y., and Gu, Z. (2018) Biodegradable 2D Fe-Al hydroxide for nanocatalytic tumor-dynamic therapy with tumor specificity. *Adv. Sci. 5*, 1801155.

(37) Qiu, M., Wang, D., Liang, W., Liu, L., Zhang, Y., Chen, X., Sang, D. K., Xing, C., Li, Z., Dong, B., et al. (2018) Novel concept of the smart NIR-light-controlled drug release of black phosphorus nanostructure for cancer therapy. *Proc. Natl. Acad. Sci. U. S. A. 115*, 501−506.

(38) Hao, J., Song, G., Liu, T., Yi, X., Yang, K., Cheng, L., and Liu, Z. (2017) *In vivo* long-term biodistribution, excretion, and toxicology of

DOI: 10.1021/acs.bioconjchem.9b00699
Bioconjugate Chem. 2020, 31, 315−331

PEGylated transition-metal dichalcogenides MS_2 (M = Mo, W, Ti) nanosheets. *Adv. Sci. 4*, 1600160.
(39) Tao, W., Ji, X., Zhu, X., Li, L., Wang, J., Zhang, Y., Saw, P. E., Li, W., Kong, N., Islam, M. A., et al. (2018) Two-dimensional antimonene-based photonic nanomedicine for cancer theranostics. *Adv. Mater. 30*, 1802061.
(40) Miao, Q., Xie, C., Zhen, X., Lyu, Y., Duan, H., Liu, X., Jokerst, J. V., and Pu, K. (2017) Molecular afterglow imaging with bright, biodegradable polymer nanoparticles. *Nat. Biotechnol. 35*, 1102−1110.
(41) Lyu, Y., Zeng, J., Jiang, Y., Zhen, X., Wang, T., Qiu, S., Lou, X., Gao, M., and Pu, K. (2018) Enhancing both biodegradability and efficacy of semiconducting polymer nanoparticles for photoacoustic imaging and photothermal therapy. *ACS Nano 12*, 1801−1810.
(42) Jiang, Y., and Pu, K. (2018) Multimodal biophotonics of semiconducting polymer nanoparticles. *Acc. Chem. Res. 51*, 1840−1849.
(43) Li, J., and Pu, K. (2019) Development of organic semiconducting materials for deep-tissue optical imaging, phototherapy and photoactivation. *Chem. Soc. Rev. 48*, 38−71.
(44) Chen, L., Chen, J., Qiu, S., Wen, L., Wu, Y., Hou, Y., Wang, Y., Zeng, J., Feng, Y., Li, Z., et al. (2018) Biodegradable nanoagents with short biological half-Life for SPECT/PAI/MRI multimodality imaging and PTT therapy of tumors. *Small 14*, 1702700.
(45) Zeng, J. F., Cheng, M., Wang, Y., Wen, L., Chen, L., Li, Z., Wu, Y. Y., Gao, M. Y., and Chai, Z. F. (2016) pH-responsive Fe(III)-gallic acid nanoparticles for *in vivo* photoacoustic imaging-guided photothermal therapy. *Adv. Healthcare Mater. 5*, 772−780.
(46) Falagan-Lotsch, P., Grzincic, E. M., and Murphy, C. J. (2017) New sdvances in nanotechnology-based diagnosis and therapeutics for breast cancer: An sssessment of active-targeting inorganic nanoplatforms. *Bioconjugate Chem. 28*, 135−152.
(47) Du, J., Zhang, X., Yan, L., and Chen, R. (2017) Functional tumor imaging based on inorganic nanomaterials. *Sci. China: Chem. 60*, 1425−1438.
(48) Wang, F., Li, C., Cheng, J., and Yuan, Z. (2016) Recent advances on inorganic nanoparticle-based cancer therapeutic agents. *Int. J. Environ. Res. Public Health 13*, 1182.
(49) Huang, H. C., Barua, S., Sharma, G., Dey, S. K., and Rege, K. (2011) Inorganic nanoparticles for cancer imaging and therapy. *J. Controlled Release 155*, 344−357.
(50) Bhattacharyya, S., Kudgus, R. A., Bhattacharya, R., and Mukherjee, P. (2011) Inorganic nanoparticles in cancer therapy. *Pharm. Res. 28*, 237−259.
(51) Cao, Z., Li, B., Sun, L., Li, L., Xu, Z. P., and Gu, Z. (2019) 2D layered double hydroxide nanoparticles: Recent progress toward preclinical/clinical Nanomedicine. *Small Methods*, 1900343.
(52) Croissant, J. G., Fatieiev, Y., and Khashab, N. M. (2017) Degradability and clearance of silicon, organosilica, silsesquioxane, silica mixed oxide, and mesoporous silica nanoparticles. *Adv. Mater. 29*, 1604634.
(53) Gulzar, A., Gai, S., Yang, P., Li, C., Ansari, M. B., and Lin, J. (2015) Stimuli responsive drug delivery application of polymer and silica in biomedicine. *J. Mater. Chem. B 3*, 8599−8622.
(54) Li, J., Duan, H., and Pu, K. (2019) Nanotransducers for near-infrared photoregulation in biomedicine. *Adv. Mater. 31*, 1901607.
(55) Luo, M., Fan, T., Zhou, Y., Zhang, H., and Mei, L. (2019) 2D black phosphorus-based biomedical applications. *Adv. Funct. Mater. 29*, 1808306.
(56) Qiu, M., Singh, A., Wang, D., Qu, J., Swihart, M., Zhang, H., and Prasad, P. N. (2019) Biocompatible and biodegradable inorganic nanostructures for nanomedicine: Silicon and black phosphorus. *Nano Today 25*, 135−155.
(57) Wang, Y., Qiu, M., Won, M., Jung, E., Fan, T., Xie, N., Chi, S., Zhang, H., and Kim, J. S. (2019) Emerging 2D material-based nanocarrier for cancer therapy beyond graphene. *Coord. Chem. Rev. 400*, 213041.
(58) Qiu, M., Ren, W. X., Jeong, T., Won, M., Park, G. Y., Sang, D. K., Liu, L. P., Zhang, H., and Kim, J. S. (2018) Omnipotent phosphorene: A next-generation, two-dimensional nanoplatform for multidisciplinary biomedical applications. *Chem. Soc. Rev. 47*, 5588−5601.
(59) Tao, W., Kong, N., Ji, X., Zhang, Y., Sharma, A., Ouyang, J., Qi, B., Wang, J., Xie, N., Kang, C., et al. (2019) Emerging two-dimensional monoelemental materials (Xenes) for biomedical applications. *Chem. Soc. Rev. 48*, 2891−2912.
(60) Yu, L., Chen, Y., Wu, M., Cai, X., Yao, H., Zhang, L., Chen, H., and Shi, J. (2016) "Manganese extraction" strategy enables tumor-sensitive biodegradability and theranostics of nanoparticles. *J. Am. Chem. Soc. 138*, 9881−9894.
(61) Wang, D., Xu, Z., Chen, Z., Liu, X., Hou, C., Zhang, X., and Zhang, H. (2014) Fabrication of single-hole glutathione-responsive degradable hollow silica nanoparticles for drug delivery. *ACS Appl. Mater. Interfaces 6*, 12600−12608.
(62) He, Q., Shi, J., Zhu, M., Chen, Y., and Chen, F. (2010) The three-stage *in vitro* degradation behavior of mesoporous silica in simulated body fluid. *Microporous Mesoporous Mater. 131*, 314−320.
(63) Hao, N., Liu, H., Li, L., Chen, D., Li, L., and Tang, F. (2012) *In vitro* degradation behavior of silica nanoparticles under physiological conditions. *J. Nanosci. Nanotechnol. 12*, 6346−6354.
(64) Arbab, A. S., Wilson, L. B., Ashari, P., Jordan, E. K., Lewis, B. K., and Frank, J. A. (2005) A model of lysosomal metabolism of dextran coated superparamagnetic iron oxide (SPIO) nanoparticles: implications for cellular magnetic resonance imaging. *NMR Biomed. 18*, 383−389.
(65) Lartigue, L., Alloyeau, D., Kolosnjaj-Tabi, J., Javed, Y., Guardia, P., Riedinger, A., Péchoux, C., Pellegrino, T., Wilhelm, C., and Gazeau, F. (2013) Biodegradation of iron oxide nanocubes: high-resolution *in situ* monitoring. *ACS Nano 7*, 3939−3952.
(66) Song, X. J., Gong, H., Yin, S. N., Cheng, L., Wang, C., Li, Z. W., Li, Y. G., Wang, X. Y., Liu, G., and Liu, Z. (2014) Ultra-small iron oxide doped polypyrrole nanoparticles for *in vivo* multimodal imaging guided photothermal therapy. *Adv. Funct. Mater. 24*, 1194−1201.
(67) Lunov, O., Syrovets, T., Roecker, C., Tron, K., Nienhaus, G. U., Rasche, V., Mailaender, V., Landfester, K., and Simmet, T. (2010) Lysosomal degradation of the carboxydextran shell of coated superparamagnetic iron oxide nanoparticles and the fate of professional phagocytes. *Biomaterials 31*, 9015−9022.
(68) Chen, Y., Yin, Q., Ji, X., Zhang, S., Chen, H., Zheng, Y., Sun, Y., Qu, H., Wang, Z., Li, Y., et al. (2012) Manganese oxide-based multifunctionalized mesoporous silica nanoparticles for pH-responsive MRI, ultrasonography and circumvention of MDR in cancer cells. *Biomaterials 33*, 7126−7137.
(69) Chen, Y., Ye, D., Wu, M., Chen, H., Zhang, L., Shi, J., and Wang, L. (2014) Break-up of two-dimensional MnO_2 nanosheets promotes ultrasensitive pH-triggered theranostics of cancer. *Adv. Mater. 26*, 7019−7026.
(70) Chen, Y., Cheng, L., Dong, Z., Chao, Y., Lei, H., Zhao, H., Wang, J., and Liu, Z. (2017) Degradable vanadium disulfide nanostructures with unique optical and magnetic functions for cancer theranostics. *Angew. Chem., Int. Ed. 56*, 12991−12996.
(71) Chen, L., Feng, Y., Zhou, X., Zhang, Q., Nie, W., Wang, W., Zhang, Y., and He, C. (2017) One-pot synthesis of MoS_2 nanoflakes with desirable degradability for photothermal cancer therapy. *ACS Appl. Mater. Interfaces 9*, 17347−17358.
(72) Zhang, Y., Ali, S. F., Dervishi, E., Xu, Y., Li, Z., Casciano, D., and Biris, A. S. (2010) Cytotoxicity effects of graphene and single-wall carbon nanotubes in neural phaeochromocytoma-derived PC12 cells. *ACS Nano 4*, 3181−3186.
(73) Allen, B. L., Kichambare, P. D., Gou, P., Vlasova, I. I., Kapralov, A. A., Konduru, N., Kagan, V. E., and Star, A. (2008) Biodegradation of single-walled carbon nanotubes through enzymatic catalysis. *Nano Lett. 8*, 3899−3903.
(74) Bianco, A., Kostarelos, K., and Prato, M. (2011) Making carbon nanotubes biocompatible and biodegradable. *Chem. Commun. 47*, 10182−10188.
(75) Michalske, T. A., and Freiman, S. W. (1983) A molecular mechanism for stress corrosion in vitreous silica. *J. Am. Ceram. Soc. 66*, 284−288.

DOI: 10.1021/acs.bioconjchem.9b00699
Bioconjugate Chem. 2020, 31, 315−331

(76) Li, X., Zhang, L., Dong, X., Liang, J., and Shi, J. (2007) Preparation of mesoporous calcium doped silica spheres with narrow size dispersion and their drug loading and degradation behavior. *Microporous Mesoporous Mater. 102*, 151−158.
(77) Popplewell, J. F., King, S. J., Day, J. P., Ackrill, P., Fifield, L. K., Cresswell, R. G., Di Tada, M. L., and Liu, K. (1998) Kinetics of uptake and elimination of silicic acid by a human subject: A novel application of ^{32}Si and accelerator mass spectrometry. *J. Inorg. Biochem. 69*, 177−180.
(78) Zhao, S., Zhang, S., Ma, J., Fan, L., Yin, C., Lin, G., and Li, Q. (2015) Double loaded self-decomposable SiO_2 nanoparticles for sustained drug release. *Nanoscale 7*, 16389−16398.
(79) Huang, P., Qian, X., Chen, Y., Yu, L., Lin, H., Wane, L., Zhu, Y., and Shi, J. (2017) Metalloporphyrin-encapsulated biodegradable nanosystems for highly efficient magnetic resonance imaging-guided sonodynamic cancer therapy. *J. Am. Chem. Soc. 139*, 1275−1284.
(80) Rogalla, S., Flisikowski, K., Gorpas, D., Mayer, A. T., Flisikowska, T., Mandella, M. J., Ma, X., Casey, K. M., Felt, S. A., Saur, D., et al. (2019) Biodegradable fluorescent nanoparticles for endoscopic detection of colorectal carcinogenesis. *Adv. Funct. Mater.*, 1904992.
(81) Pohaku Mitchell, K. K., Liberman, A., Kummel, A. C., and Trogler, W. C. (2012) Iron(III)-doped, silica nanoshells: A biodegradable form of silica. *J. Am. Chem. Soc. 134*, 13997−14003.
(82) Peng, Y. K., Liu, C. L., Chen, H. C., Chou, S. W., Tseng, W. H., Tseng, Y. J., Kang, C. C., Hsiao, J. K., and Chou, P. T. (2013) Antiferromagnetic iron nanocolloids: A new generation *in vivo* T_1 MRI contrast agent. *J. Am. Chem. Soc. 135*, 18621−18628.
(83) Kolosnjaj-Tabi, J., Javed, Y., Lartigue, L., Volatron, J., Elgrabli, D., Marangon, I., Pugliese, G., Caron, B., Figuerola, A., Luciani, N., et al. (2015) The one year fate of iron oxide coated gold nanoparticles in mice. *ACS Nano 9*, 7925−7939.
(84) Liu, Y., Zhang, G., Guo, Q., Ma, L., Jia, Q., Liu, L., and Zhou, J. (2017) Artificially controlled degradable inorganic nanomaterial for cancer theranostics. *Biomaterials 112*, 204−217.
(85) Wu, C., Wang, S., Zhao, J., Liu, Y., Zheng, Y., Luo, Y., Ye, C., Huang, M., and Chen, H. (2019) Biodegradable Fe(III)@WS_2-PVP nanocapsules for redox reaction and TME-enhanced nanocatalytic, hotothermal, and chemotherapy. *Adv. Funct. Mater. 29*, 1901722.
(86) Farrera, C., Bhattacharya, K., Lazzaretto, B., Andon, F. T., Hultenby, K., Kotchey, G. P., Star, A., and Fadeel, B. (2014) Extracellular entrapment and degradation of single-walled carbon nanotubes. *Nanoscale 6*, 6974−6983.
(87) Zhao, Y., Allen, B. L., and Star, A. (2011) Enzymatic degradation of multiwalled carbon nanotubes. *J. Phys. Chem. A 115*, 9536−9544.
(88) Peng, Y. K., Tseng, Y. J., Liu, C. L., Chou, S. W., Chen, Y. W., Tsang, S. C. E., and Chou, P. T. (2015) One-step synthesis of degradable T_1-FeOOH functionalized hollow mesoporous silica nanocomposites from mesoporous silica spheres. *Nanoscale 7*, 2676−2687.
(89) Wang, S., Yang, L., Cho, H., Dean Chueng, S., Zhang, H., Zhang, Q., and Lee, K. (2019) Programmed degradation of a hierarchical nanoparticle with redox and light responsivity for self-activated photo-chemical enhanced chemodynamic therapy. *Biomaterials 224*, 119498−119498.
(90) Chen, Q., Feng, L., Liu, J., Zhu, W., Dong, Z., Wu, Y., and Liu, Z. (2016) Intelligent albumin-MnO_2 nanoparticles as pH-/H_2O_2-responsive dissociable nanocarriers to modulate tumor hypoxia for effective combination therapy. *Adv. Mater. 28*, 7129−7136.
(91) Dai, Y., Xu, C., Sun, X., and Chen, X. (2017) Nanoparticle design strategies for enhanced anticancer therapy by exploiting the tumour microenvironment. *Chem. Soc. Rev. 46*, 3830−3852.
(92) Chen, D., Zhang, G., Li, R., Guan, M., Wang, X., Zou, T., Zhang, Y., Wang, C., Shu, C., Hong, H., et al. (2018) Biodegradable, hydrogen peroxide, and glutathione dual responsive nanoparticles for potential programmable paclitaxel release. *J. Am. Chem. Soc. 140*, 7373−7376.
(93) Zhu, M. T., Feng, W. Y., Wang, Y., Wang, B., Wang, M., Ouyang, H., Zhao, Y. L., and Chai, Z. F. (2009) Particokinetics and extrapulmonary translocation of intratracheally instilled ferric oxide nanoparticles in rats and the potential health risk assessment. *Toxicol. Sci. 107*, 342−351.
(94) Chen, F., Goel, S., Valdovinos, H. F., Luo, H. M., Hernandez, R., Barnhart, T. E., and Cai, W. B. (2015) *In vivo* integrity and biological fate of chelator-Free zirconium-89-labeled mesoporous silica nanoparticles. *ACS Nano 9*, 7950−7959.
(95) Chen, G. T., Teng, Z. G., Su, X. D., Liu, Y., and Lu, G. M. (2015) Unique biological degradation behavior of stober mesoporous silica nanoparticles from their interiors to their exteriors. *J. Biomed. Nanotechnol. 11*, 722−729.
(96) Mei, L., Zhang, X., Yin, W., Dong, X., Guo, Z., Fu, W., Su, C., Gu, Z., and Zhao, Y. (2019) Translocation, biotransformation-related degradation, and toxicity assessment of polyvinylpyrrolidone-modified 2H-phase nano-MoS_2. *Nanoscale 11*, 4767−4780.
(97) Kim, B. H., Lee, N., Kim, H., An, K., Park, Y. I., Choi, Y., Shin, K., Lee, Y., Kwon, S. G., Na, H. B., et al. (2011) Large-scale synthesis of uniform and extremely small-sized iron oxide nanoparticles for high-resolution T_1 magnetic resonance imaging contrast agents. *J. Am. Chem. Soc. 133*, 12624−12631.
(98) Li, Z., Wei, L., Gao, M. Y., and Lei, H. (2005) One-pot reaction to synthesize biocompatible magnetite nanoparticles. *Adv. Mater. 17*, 1001−1005.
(99) Hu, F. Q., Wei, L., Zhou, Z., Ran, Y. L., Li, Z., and Gao, M. Y. (2006) Preparation of biocompatible magnetite nanocrystals for *in vivo* magnetic resonance detection of cancer. *Adv. Mater. 18*, 2553−2556.
(100) Lee, N., Choi, Y., Lee, Y., Park, M., Moon, W. K., Choi, S. H., and Hyeon, T. (2012) Water-dispersible ferrimagnetic iron oxide nanocubes with extremely high r_2 relaxivity for highly sensitive *in vivo* MRI of tumors. *Nano Lett. 12*, 3127−3131.
(101) Gao, Z., Hou, Y., Zeng, J., Chen, L., Liu, C., Yang, W., and Gao, M. (2017) Tumor microenvironment-triggered aggregation of antiphagocytosis ^{99m}Tc-labeled Fe_3O_4 nanoprobes for enhanced tumor imaging *in vivo*. *Adv. Mater. 29*, 1701095.
(102) Ma, T., Hou, Y., Zeng, J., Liu, C., Zhang, P., Jing, L., Shangguan, D., and Gao, M. (2018) Dual-ratiometric target-triggered fluorescent probe for simultaneous quantitative visualization of tumor microenvironment protease activity and pH *in Vivo*. *J. Am. Chem. Soc. 140*, 211−218.
(103) Ma, N., Zhang, M. K., Wang, X. S., Zhang, L., Feng, J., and Zhang, X. Z. (2018) NIR light-triggered degradable $MoTe_2$ nanosheets for combined photothermal and chemotherapy of cancer. *Adv. Funct. Mater. 28*, 1801139.
(104) Ji, X., Kong, N., Wang, J., Li, W., Xiao, Y., Gan, S. T., Zhang, Y., Li, Y., Song, X., Xiong, Q., et al. (2018) A novel top-down synthesis of ultrathin 2D boron nanosheets for multimodal imaging-guided cancer therapy. *Adv. Mater. 30*, 1803031.
(105) Xue, T., Liang, W., Li, Y., Sun, Y., Xiang, Y., Zhang, Y., Dai, Z., Duo, Y., Wu, L., Qi, K., et al. (2019) Ultrasensitive detection of miRNA with an antimonene-based surface plasmon resonance sensor. *Nat. Commun. 10*, 28.
(106) Xing, C., Chen, S., Liang, X., Liu, Q., Qu, M., Zou, Q., Li, J., Tan, H., Liu, L., Fan, D., et al. (2018) Two-dimensional MXene (Ti_3C_2)-integrated cellulose hydrogels: Toward smart three-dimensional network nanoplatforms exhibiting light-induced swelling and bimodal photothermal/chemotherapy anticancer activity. *ACS Appl. Mater. Interfaces 10*, 27631−27643.
(107) Xing, C., Chen, S., Qiu, M., Liang, X., Liu, Q., Zou, Q., Li, Z., Xie, Z., Wang, D., Dong, B., et al. (2018) Conceptually novel black phosphorus/cellulose hydrogels as promising photothermal agents for effective cancer therapy. *Adv. Healthcare Mater. 7*, 1701510.
(108) Xing, C., Jing, G., Liang, X., Qiu, M., Li, Z., Cao, R., Li, X., Fan, D., and Zhang, H. (2017) Graphene oxide/black phosphorus nanoflake aerogels with robust thermo-stability and significantly enhanced photothermal properties in air. *Nanoscale 9*, 8096−8101.

DOI: 10.1021/acs.bioconjchem.9b00699
Bioconjugate Chem. 2020, 31, 315−331

(109) Zhou, L., Chen, Z., Dong, K., Yin, M., Ren, J., and Qu, X. (2014) DNA-mediated biomineralization of rare-earth nanoparticles for simultaneous imaging and stimuli-responsive drug delivery. *Biomaterials 35*, 8694−8702.
(110) Liu, J.-F., Wei, L., Duolikun, D., Hou, X.-D., Chen, F., Liu, J.-J., and Zheng, L.-P. (2018) Preparation of porous calcium phosphate microspheres with phosphate-containing molecules at room temperature for drug delivery and osteogenic differentiation. *RSC Adv. 8*, 25480−25488.
(111) Yu, W., Sun, T., Qi, C., Ding, Z., Zhao, H., Chen, F., Chen, D., Zhu, Y., Shi, Z., and He, Y. (2017) Strontium-doped amorphous calcium phosphate porous microspheres synthesized through a microwave-hydrothermal method using fructose 1,6-Bisphosphate as an organic phosphorus source: Application in drug delivery and enhanced bone regeneration. *ACS Appl. Mater. Interfaces 9*, 3306−3317.
(112) Zhou, Z. F., Sun, T. W., Chen, F., Zuo, D. Q., Wang, H. S., Hua, Y. Q., Cai, Z. D., and Tan, J. (2017) Calcium phosphate-phosphorylated adenosine hybrid microspheres for anti-osteosarcoma drug delivery and osteogenic differentiation. *Biomaterials 121*, 1−14.
(113) Lee, D., Beack, S., Yoo, J., Kim, S.-K., Lee, C., Kwon, W., Hahn, S. K., and Kim, C. (2018) *In vivo* photoacoustic imaging of livers using biodegradable hyaluronic acid-conjugated silica nanoparticles. *Adv. Funct. Mater. 28*, 1800941.
(114) Li, H., Li, K., Dai, Y., Xu, X., Cao, X., Zeng, Q., He, H., Pang, L., Liang, J., Chen, X., et al. (2018) *In vivo* near infrared fluorescence imaging and dynamic quantification of pancreatic metastatic tumors using folic acid conjugated biodegradable mesoporous silica nanoparticles. *Nanomedicine 14*, 1867−1877.
(115) Park, Y., Yoo, J., Kang, M. H., Kwon, W., and Joo, J. (2019) Photoluminescent and biodegradable porous silicon nanoparticles for biomedical imaging. *J. Mater. Chem. B 7*, 6259−6460.
(116) Zhang, S., Chu, Z., Yin, C., Zhang, C., Lin, G., and Li, Q. (2013) Controllable drug release and simultaneously carrier decomposition of SiO_2-drug composite nanoparticles. *J. Am. Chem. Soc. 135*, 5709−5716.
(117) Yamada, H., Urata, C., Aoyama, Y., Osada, S., Yamauchi, Y., and Kuroda, K. (2012) Preparation of colloidal mesoporous silica nanoparticles with different diameters and their unique degradation behavior in static aqueous systems. *Chem. Mater. 24*, 1462−1471.
(118) Shen, D., Yang, J., Li, X., Zhou, L., Zhang, R., Li, W., Chen, L., Wang, R., Zhang, F., and Zhao, D. (2014) Biphase stratification approach to three-dimensional dendritic biodegradable mesoporous silica nanospheres. *Nano Lett. 14*, 923−932.
(119) Hadipour Moghaddam, S. P., Mohammadpour, R., and Ghandehari, H. (2019) *In vitro* and *in vivo* evaluation of degradation, toxicity, biodistribution, and clearance of silica nanoparticles as a function of size, porosity, density, and composition. *J. Controlled Release 311−312*, 1−15.
(120) He, Q., Zhang, Z., Gao, F., Li, Y., and Shi, J. (2011) *In vivo* biodistribution and urinary excretion of mesoporous silica nanoparticles: Effects of particle size and PEGylation. *Small 7*, 271−280.
(121) Cauda, V., Argyo, C., and Bein, T. (2010) Impact of different PEGylation patterns on the long-term bio-stability of colloidal mesoporous silica nanoparticles. *J. Mater. Chem. 20*, 8693−8699.
(122) Hao, X., Hu, X., Zhang, C., Chen, S., Li, Z., Yang, X., Liu, H., Jia, G., Liu, D., Ge, K., et al. (2015) Hybrid mesoporous silica-based drug carrier nanostructures with improved degradability by hydroxyapatite. *ACS Nano 9*, 9614−9625.
(123) Shi, M., Chen, Z., Farnaghi, S., Friis, T., Mao, X., Xiao, Y., and Wu, C. (2016) Copper-doped mesoporous silica nanospheres, a promising immunomodulatory agent for inducing osteogenesis. *Acta Biomater. 30*, 334−344.
(124) Huang, X., Li, L., Liu, T., Hao, N., Liu, H., Chen, D., and Tang, F. (2011) The shape effect of mesoporous silica nanoparticles on biodistribution, clearance, and biocompatibility *in vivo*. *ACS Nano 5*, 5390−5399.
(125) Lu, Y., Xu, Y., Zhang, G., Ling, D., Wang, M., Zhou, Y., Wu, Y., Wu, T., Hackett, M. J., Hyo Kim, B., et al. (2017) Iron oxide nanoclusters for T_1 magnetic resonance imaging of non-human primates. *Nat. Biomed. Eng. 1*, 637−643.
(126) Gao, Z., Ma, T., Zhao, E., Docter, D., Yang, W., Stauber, R. H., and Gao, M. (2016) Small is smarter: Nano MRI contrast agents-advantages and recent achievements. *Small 12*, 556−576.
(127) Lee, N., and Hyeon, T. (2012) Designed synthesis of uniformly sized iron oxide nanoparticles for efficient magnetic resonance imaging contrast agents. *Chem. Soc. Rev. 41*, 2575−2589.
(128) Kumar, C., and Mohammad, F. (2011) Magnetic nanomaterials for hyperthermia-based therapy and controlled drug delivery. *Adv. Drug Delivery Rev. 63*, 789−808.
(129) Laurent, S., Dutz, S., Hafeli, U. O., and Mahmoudi, M. (2011) Magnetic fluid hyperthermia: Focus on superparamagnetic iron oxide nanoparticles. *Adv. Colloid Interface Sci. 166*, 8−23.
(130) Sonvico, F., Mornet, S., Vasseur, S., Dubernet, C., Jaillard, D., Degrouard, J., Hoebeke, J., Duguet, E., Colombo, P., and Couvreur, P. (2005) Folate-conjugated iron oxide nanoparticles for solid tumor targeting as potential specific magnetic hyperthermia mediators: Synthesis, physicochemical characterization, and *in vitro* experiments. *Bioconjugate Chem. 16*, 1181−1188.
(131) Jia, Q. J., Zeng, J. F., Qjao, R. R., Jing, L. H., Peng, L., Gu, F. L., and Gao, M. Y. (2011) Gelification: An effective measure for achieving differently sized biocompatible Fe_3O_4 nanocrystals through a single preparation recipe. *J. Am. Chem. Soc. 133*, 19512−19523.
(132) Park, J., An, K. J., Hwang, Y. S., Park, J. G., Noh, H. J., Kim, J. Y., Park, J. H., Hwang, N. M., and Hyeon, T. (2004) Ultra-large-scale syntheses of monodisperse nanocrystals. *Nat. Mater. 3*, 891−895.
(133) Wei, H., Bruns, O. T., Kaul, M. G., Hansen, E. C., Barch, M., Wiśniowska, A., Chen, O., Chen, Y., Li, N., Okada, S., et al. (2017) Exceedingly small iron oxide nanoparticles as positive MRI contrast agents. *Proc. Natl. Acad. Sci. U. S. A. 114*, 2325−2330.
(134) Zhou, Z., Zhu, X., Wu, D., Chen, Q., Huang, D., Sun, C., Xin, J., Ni, K., and Gao, J. (2015) Anisotropic shaped iron oxide nanostructures: Controlled synthesis and proton relaxation shortening effects. *Chem. Mater. 27*, 3505−3515.
(135) Zeng, J. F., Jing, L. H., Hou, Y., Jiao, M. X., Qiao, R. R., Jia, Q. J., Liu, C. Y., Fang, F., Lei, H., and Gao, M. Y. (2014) Anchoring group effects of surface ligands on magnetic properties of Fe_3O_4 nanoparticles: Towards high performance MRI contrast agents. *Adv. Mater. 26*, 2694−2698.
(136) Pöselt, E., Kloust, H., Tromsdorf, U., Janschel, M., Hahn, C., Maßlo, C., and Weller, H. (2012) Relaxivity optimization of a PEGylated iron-oxide-based negative magnetic resonance contrast agent for T_2-Weighted spin-echo imaging. *ACS Nano 6*, 1619−1624.
(137) Thorek, D. L. J., Ulmert, D., Diop, N. F. M., Lupu, M. E., Doran, M. G., Huang, R. M., Abou, D. S., Larson, S. M., and Grimm, J. (2014) Non-invasive mapping of deep-tissue lymph nodes in live animals using a multimodal PET/MRI nanoparticle. *Nat. Commun. 5*, 3097.
(138) Torres Martin de Rosales, R., Tavare, R., Glaria, A., Varma, G., Protti, A., and Blower, P. J. (2011) ^{99m}Tc-bisphosphonate-iron oxide nanoparticle conjugates for dual-modality biomedical imaging. *Bioconjugate Chem. 22*, 455−465.
(139) Cha, E. J., Jang, E. S., Sun, I. C., Lee, I. J., Ko, J. H., Kim, Y. I., Kwon, I. C., Kim, K., and Ahn, C. H. (2011) Development of MRI/NIRF 'activatable' multimodal imaging probe based on iron oxide nanoparticles. *J. Controlled Release 155*, 152−158.
(140) Guzman, R., Uchida, N., Bliss, T. M., He, D. P., Christopherson, K. K., Stellwagen, D., Capela, A., Greve, J., Malenka, R. C., Moseley, M. E., et al. (2007) Long-term monitoring of transplanted human neural stem cells in developmental and pathological contexts with MRI. *Proc. Natl. Acad. Sci. U. S. A. 104*, 10211−10216.
(141) Li, L., Jiang, W., Luo, K., Song, H. M., Lan, F., Wu, Y., and Gu, Z. W. (2013) Superparamagnetic iron oxide nanoparticles as MRI contrast agents for non-invasive stem cell labeling and tracking. *Theranostics 3*, 595−615.
(142) Theruvath, A. J., Nejadnik, H., Muehe, A. M., Gassert, F., Lacayo, N. J., Goodman, S. B., and Daldrup-Link, H. E. (2018)

DOI: 10.1021/acs.bioconjchem.9b00699
Bioconjugate Chem. 2020, 31, 315−331

Tracking cell transplants in femoral osteonecrosis with magnetic resonance imaging: A proof-of-concept study in patients. *Clin. Cancer Res. 24*, 6223−6229.
(143) Llop, J., Jiang, P., Marradi, M., Gomez-Vallejo, V., Echeverria, M., Yu, S., Puigivila, M., Baz, Z., Szczupak, B., Perez-Campana, C., et al. (2015) Visualisation of dual radiolabelled poly(lactide-*co*-glycolide) nanoparticle degradation *in vivo* using energy-discriminant SPECT. *J. Mater. Chem. B 3*, 6293−6300.
(144) Zeng, J. F., Jia, B., Qiao, R. R., Wang, C., Jing, L. H., Wang, F., and Gao, M. Y. (2014) *In situ* ^{111}In-doping for achieving biocompatible and non-leachable ^{111}In-labeled Fe_3O_4 nanoparticles. *Chem. Commun. 50*, 2170−2172.
(145) Levy, M., Lagarde, F., Maraloiu, V. A., Blanchin, M. G., Gendron, F., Wilhelm, C., and Gazeau, F. (2010) Degradability of superparamagnetic nanoparticles in a model of intracellular environment: Follow-up of magnetic, structural and chemical properties. *Nanotechnology 21*, 395103.
(146) Levy, M., Luciani, N., Alloyeau, D., Elgrabli, D., Deveaux, V., Pechoux, C., Chat, S., Wang, G., Vats, N., Gendron, F., et al. (2011) Long term *in vivo* biotransformation of iron oxide nanoparticles. *Biomaterials 32*, 3988−3999.
(147) Kolosnjaj-Tabi, J., Di Corato, R., Lartigue, L., Marangon, I., Guardia, P., Silva, A. K. A., Luciani, N., Clément, O., Flaud, P., Singh, J. V., et al. (2014) Heat-generating iron oxide nanocubes: Subtle "destructurators" of the tumoral microenvironment. *ACS Nano 8*, 4268−4283.
(148) Yang, G., Xu, L., Chao, Y., Xu, J., Sun, X., Wu, Y., Peng, R., and Liu, Z. (2017) Hollow MnO_2 as a tumor-microenvironment-responsive biodegradable nano-platform for combination therapy favoring antitumor immune responses. *Nat. Commun. 8*, 902.
(149) Fan, H., Yan, G., Zhao, Z., Hu, X., Zhang, W., Liu, H., Fu, X., Fu, T., Zhang, X., and Tan, W. (2016) A smart photosensitizer-MnO_2 nanosystem for enhanced photodynamic therapy by reducing glutathione levels in cancer cells. *Angew. Chem., Int. Ed. 55*, 5477−5482.
(150) Wang, X., Niu, D. C., Wu, Q., Bao, S., Su, T., Liu, X. H., Zhang, S. J., and Wang, Q. G. (2015) Iron oxide/manganese oxide co-loaded hybrid nanogels as pH-responsive magnetic resonance contrast agents. *Biomaterials 53*, 349−357.
(151) Tan, C. L., and Zhang, H. (2015) Two-dimensional transition metal dichalcogenide nanosheet-based composites. *Chem. Soc. Rev. 44*, 2713−2731.
(152) Lin, J., Chen, X. Y., and Huang, P. (2016) Graphene-based nanomaterials for bioimaging. *Adv. Drug Delivery Rev. 105*, 242−254.
(153) Goenka, S., Sant, V., and Sant, S. (2014) Graphene-based nanomaterials for drug delivery and tissue engineering. *J. Controlled Release 173*, 75−88.
(154) Donaldson, K., Poland, C. A., Murphy, F. A., MacFarlane, M., Chernova, T., and Schinwald, A. (2013) Pulmonary toxicity of carbon nanotubes and asbestos - Similarities and differences. *Adv. Drug Delivery Rev. 65*, 2078−2086.
(155) Murray, A. R., Kisin, E., Leonard, S. S., Young, S. H., Kommineni, C., Kagan, V. E., Castranova, V., and Shvedova, A. A. (2009) Oxidative stress and inflammatory response in dermal toxicity of single-walled carbon nanotubes. *Toxicology 257*, 161−171.
(156) Allen, B. L., Kotchey, G. P., Chen, Y. N., Yanamala, N. V. K., Klein-Seetharaman, J., Kagan, V. E., and Star, A. (2009) Mechanistic investigations of horseradish peroxidase-catalyzed degradation of single-walled carbon nanotubes. *J. Am. Chem. Soc. 131*, 17194−17205.
(157) Kurapati, R., Russier, J., Squillaci, M. A., Treossi, E., Menard-Moyon, C., Del Rio-Castillo, A. E., Vazquez, E., Samori, P., Palermo, V., and Bianco, A. (2015) Dispersibility-dependent biodegradation of graphene oxide by myeloperoxidase. *Small 11*, 3985−3994.
(158) Huang, X., Andina, D., Ge, J., Labarre, A., Leroux, J. C., and Castagner, B. (2017) Characterization of calcium phosphate nanoparticles based on a PEGylated chelator for gene delivery. *ACS Appl. Mater. Interfaces 9*, 10435−10445.
(159) Boyjoo, Y., Pareek, V. K., and Liu, J. (2014) Synthesis of micro and nano-sized calcium carbonate particles and their applications. *J. Mater. Chem. A 2*, 14270−14288.
(160) Wang, C., Liu, X., Chen, S., Hu, F., Sun, J., and Yuan, H. (2018) Facile preparation of phospholipid-amorphous calcium carbonate hybrid nanoparticles: toward controllable burst drug release and enhanced tumor penetration. *Chem. Commun. 54*, 13080−13083.
(161) Zhao, Y., Wang, H., Huang, H., Xiao, Q., Xu, Y., Guo, Z., Xie, H., Shao, J., Sun, Z., Han, W., et al. (2016) Surface coordination of black phosphorus for robust air and water stability. *Angew. Chem., Int. Ed. 55*, 5003−5007.
(162) Lin, H., Gao, S., Dai, C., Chen, Y., and Shi, J. (2017) A two-dimensional biodegradable niobium carbide (MXene) for photothermal tumor eradication in NIR-I and NIR-II biowindows. *J. Am. Chem. Soc. 139*, 16235−16247.
(163) Cheng, L., Wang, X., Gong, F., Liu, T., and Liu, Z. (2019) 2D nanomaterials for cancer theranostic applications. *Adv. Mater.*, 1902333.
(164) Dorozhkin, S. V., and Epple, M. (2002) Biological and medical significance of calcium phosphates. *Angew. Chem., Int. Ed. 41*, 3130−3146.
(165) Doerdelmann, G., Kozlova, D., Karczewski, S., Lizio, R., Knauer, S., and Epple, M. (2014) Calcium phosphate increases the encapsulation efficiency of hydrophilic drugs (proteins, nucleic acids) into poly($_{D,L}$-lactide-*co*-glycolide acid) nanoparticles for intracellular delivery. *J. Mater. Chem. B 2*, 7250−7259.
(166) Lee, D., Upadhye, K., and Kumta, P. N. (2012) Nano-sized calcium phosphate (CaP) carriers for non-viral gene delivery. *Mater. Sci. Eng., B 177*, 289−302.
(167) Chen, F., Huang, P., Qi, C., Lu, B., Zhao, X., Li, C., Wu, J., Cui, D., and Zhu, Y. (2014) Multifunctional biodegradable mesoporous microspheres of Eu^{3+}-doped amorphous calcium phosphate: Microwave-assisted preparation, pH-sensitive drug release, and bioimaging application. *J. Mater. Chem. B 2*, 7132−7140.
(168) Sun, C., Wen, L., Zeng, J., Wang, Y., Sun, Q., Deng, L., Zhao, C., and Li, Z. (2016) One-pot solventless preparation of PEGylated black phosphorus nanoparticles for photoacoustic imaging and photothermal therapy of cancer. *Biomaterials 91*, 81−89.
(169) Huang, J., Li, J., Lyu, Y., Miao, Q., and Pu, K. (2019) Molecular optical imaging probes for early diagnosis of drug-induced acute kidney injury. *Nat. Mater. 18*, 1133−1143.
(170) Huang, J., Xie, C., Zhang, X., Jiang, Y., Li, J., Fan, Q., and Pu, K. (2019) Renal-clearable molecular semiconductor for second near-infrared fluorescence imaging of kidney dysfunction. *Angew. Chem., Int. Ed. 58*, 15120−15127.

DOI: 10.1021/acs.bioconjchem.9b00699
Bioconjugate Chem. 2020, 31, 315−331